POLITECNICO DI TORINO

Department of Electronics and Telecommunications

Master Degree in Telecommunications Engineering

Master Degree Thesis

Accumulation of the non linear interference in optical links

Supervisor: Prof. CURRI VITTORIO

Co-supervisor: Dr. PILORI DARIO Dr. CANTONO MATTIA

Candidate: CHENG QIAN(213724)

NOVEMBER 2019

Contents

Abstract

With the deepening of society information, the IP services, as a representative of data services, have an explosive growth. As a result, the field of communication has developed rapidly. New communication technologies and new programs have sprung up. But, there are also numerous problems in it. Application of new technologies can solve a particular aspect of the problem, but coming with other problems inevitably. If these problems are not solved appropriately, the results of accumulation are the declining of the system performance and the increasing of the system cost, restricting the increasing of the communication capacity and can't meet people's growing needs of communication capacity.

Compared to the cable communication, the fiber communication has greater transmission capacity, longer transmission distance and stronger anti-jamming capability, so it has became the development trend of the communication technology. In the developing process of the fiber communication, the wavelength division multiplexing technology came into being. There is only one way of signal in one fiber in the past fiber communication systems. So, more fibers should be lay in order to increase the capacity of the system, it makes the cost go up significantly(3). But the wavelength division multiplexing technology can achieve contemporary transmission of multiple signals in the same fiber,

which can increase the system capacity significantly, so it has been considered as an effective method to solve the communication capacity problem. But, as been said before, the application of new technology will inevitably come with new problems, including group velocity dispersion (GVD), polarization mode dispersion (PMD) , the amplifier noise, transient effect, the channel crosstalk and fiber non-linearity(18). The channel spacing is becoming smaller and smaller in order to increase the system capacity in WDM system, which causes the channel crosstalk problem in the system getting worse. This article is focused on the study of the channel crosstalk problem. The main works lie:

Understand that the accumulation of Non linear interference in optical fiber transmission can improve performance better. In this thesis, We studied the characteristics of nonlinear interference noise (NLIN) in fiber communication systems with large cumulative dispersion. Frequency domain and time domain analysis were published, which attributed very different attributes to NLIN. After reviewing the two methods, we have identified some reasonable assumptions that are key to the GN model derivation and are reasonable. We perform extensive simulation verification by solving a number of rich and important formats including PM-BPSK, PM-QPSK, PM-8QAM and PM-16QAM, We have multiple values for all three different types of fiber (PSCF, SMF and NZDSF) and WDM channel spacing(5). We derived the true NLIN

power and verified that NLIN is additive Gaussian. It was upgraded to enhanced GN model or EGN model. In addition, we focus on the other part of non linear propagation, which is symbol rate, long-term correlation and non-linearity formats.

Keyword: Coherent systems, GN model, EGN model, IGN model, PM-QAM, PM-BPSK, PM-QPSK, Uncompensated transmission, Nonlinear interference, Nyquist-WDM

Chapter 1 Introduction

In the recent years the ultra distance optical links is very paid attention in the world. They benefit from the rapid development of coherent detection systems. and also they were achieving ever increasing performance records.

Reducing the channel spacing is an effective means to improve the spectral efficiency. As the channel spacing decreases, the signal spectrum in different channels of the same fiber in the system will be spectrally aliased, and the same-frequency crosstalk problem will appear, non linear interference is a important indicator in the ultra distance optical links. The distortion of the spectrum causes the bit error rate of the receiving end to increase, which makes it difficult for the receiving end to recover the original signal, which becomes a major factor that restricts the system capacity increase.

Section 1 The system of the optical transmission

The overall structure of the N-channel wavelength-multiplexed WDM system is mainly composed of three parts: the transmitting and receiving optical multiplexing terminal (OMT) unit and the trunking line developed (ILA) unit(1).

(1) Optical wavelength conversion unit (OTU);

(2) Wavelength division multiplexer: split/combiner (ODU/OMU);

(3) Optical amplifier (BA/LA/PA);

(4) Optical monitoring channel/channel (OSC);

The Optical Wavelength Conversion Unit (OTU) converts non-standard wavelengths into standard wavelengths specified by ITU-T. The optical/electrical/optical (O/E/O) conversion is applied in the system, ie, the photodiode PIN or APD is used first(1). The received optical signal is converted to an electrical signal, which is then modulated by a standard wavelength laser to obtain a new desired optical wavelength signal(1). The wavelength division multiplexer can be divided into an optical multiplexer at the transmitting end and an optical splitter at the receiving end. The optical multiplexer is used for the transmitting end of the transmission system(1). It is a device with multiple input ports and one output port. Each input port inputs a per-selected wavelength optical signal, and the input different wavelengths of light waves are output by the same output port. The optical demultiplexer is used at the receiving end of the transmission system, just opposite to the optical combiner. It has an input port and multiple output ports to classify multiple different wavelength signals(1). The optical amplifier not only directly amplifies the optical signal, but also has real-time, high-gain, wide-band, online, low-noise, low-loss all-optical amplifier, which is an indispensable key component in the new generation of optical fiber communication systems. Among the currently practical fiber amplifiers are erbium-doped fiber

amplifiers (EDFAs), semiconductor optical amplifiers (SOAs), and fiber Raman amplifiers (FRAs)(4). Among them, erbium-doped fiber amplifiers are widely used for long distances due to their superior performance. In high-capacity, high-speed optical fiber communication systems, it is used as a per-amplifier, line amplifier, and power amplifier(4).

The optical supervisory channel is established for the monitoring of the WDM optical transmission system. ITU-T recommends a 1510nm wavelength with a capacity of 2Mbit/s (1). High receiver sensitivity (better than -50dBm) at low speeds still works. However, the light path must be taken before the EDFA and the light path after the EDFA.

Section 2 Working principle of optical transmission system

Optical fiber has huge bandwidth resources. However, due to technical factors and other factors, people can only use a small part of it. Wavelength division multiplexing technology has solved this problem well. It is a kind of fiber low loss area. Communication technology that makes full use of bandwidth resources. Wavelength division multiplexing technology divides the low loss region of the fiber into multiple paths according to the wavelength of the transmitted light wave, and uses the light wave with different wavelengths as the carrier of the signal. Each channel is regarded as a channel and can be transmitted with specific

Optical carrier signal of wavelength. In the transmission process, optical carrier signals of different wavelengths are transmitted in channels divided into different frequency bands, so that the optical carrier signal transmission processes can be regarded as independent of each other without considering the non-linearity of the optical fibers. Just as optical carrier signals are transmitted in different fibers before wavelength division multiplexing occurs, simultaneous transmission of multiple signals in a single fiber is possible. For the problem of how to realize bidirectional transmission, it is only necessary to separately modulate signals in two directions to transmit channels in different wavelengths. The number of reusable waves in a wavelength division multiplexing system depends mainly on the optical carrier frequency spacing allowed by the designed wavelength division multiplexer and demultiplexer. At present, commercial wavelength division multiplexing systems can be multiplexed with wavelengths of 16, 32, 64, etc.

The wavelength division multiplexing technology is implemented as follows: First, at the transmitting end of the system, the multi-channel signal is modulated onto the optical carrier of different wavelengths by up-conversion, and the optical carrier signal carries all the information of the original signal, and then passes the wavelength division multiplexing. The optical carrier signals having different wavelengths are coupled to a plurality of previously defined paths in the same optical fiber for

transmission. In the transmission process, due to the optical fiber transmission loss, a transmission amplifier is used to transmit signals at a certain distance. Amplification (currently used as an erbium-doped fiber amplifier) for long-distance transmission; then, at the receiving end of the system, the wave-demultiplexing multiplexer is used to demultiplex the transmitted signals in the fiber(1), coupling these together Optical carriers having different wavelengths and carrying different signals are separated; finally, the separated optical carrier signals are down-converted, and the decision circuit is used to restore the original signals, thereby finally realizing the transmission of multiple signals. After analyzing the working principle of the wavelength division multiplexing system, we can see that the wavelength division multiplexing technology is actually the frequency division multiplexing technology in the optical domain(3), which performs the transmission bandwidth of the low loss region of the optical fiber in the frequency domain. The split mode is divided into multiple sub-channels, so that the optical carrier signal of each specific wavelength is transmitted in one sub-channel and occupies a specific bandwidth in the optical fiber, which is more technical than the frequency division multiplexing technology of the coaxial cable that has been used in the past. The difference is:

(1) The difference in transmission medium. Wavelength division multiplexing technology divides the fiber bandwidth by frequency in the

optical domain, while coaxial Cable frequency division multiplexing technology implements frequency division on the electrical domain.

(2) The types of signals transmitted in the system are different. The wavelength division multiplexing system transmits digital signals, while the coaxial cable frequency division multiplexing system transmits analog voice signals with a bandwidth of 4 kHz(14).

Section 3 The structure of this thesis

The thesis is structured as follows:

In chapter 2, we introduce the Non linear interference noise, classify of the the no linear interference and how the no linear interference can be accumulated in the optical links

Then, in chapter 3, we will review the basic knowledge and background of frequency domain model and we will review the family of the frequency domain model, e the family of the GN-model, in this chapter we introduce the derivation and configuration of GN-model and the modeling signal in this model. And also we introduction what is the IGN-model and EGN-model.

In chapter 4, we review the family of the time domain model. In this chapter we will introduce the theory of the TD models and the difference part with FD models.

In chapter 5, we compare the performance between frequency

domain models and time domain models. We also introduce the different performance of the IGN model and EGN model with GN model.

In Section 6, we present a physical simulation environment for open optical transmission on telecommunications infrastructure projects for the design and operation of transmission quality assessments.

In Section 7, we conclusion the result of all the models and to analytical the different performance between different models.

Chapter 2 Non linear interference noise

Crosstalk in WDM systems has become an important factor affecting the performance of their systems. There are many types of crosstalk in WDM systems, and the terminology for crosstalk description is also different. From the physical mechanism of crosstalk generation, crosstalk in WDM systems can be roughly divided into linear interference and non linear interference. In a WDM system, the sum of the energy of each channel constitutes the total energy of the fiber transmission. Therefore, even if the energy of each channel is not large, as the number of multiplexed channels in the system increases, the total energy transmitted in the fiber will also A large value is reached, and with the increase in energy, the nonlinear effects in the light continue to deteriorate and deteriorate. The main causes of crosstalk between channels in nonlinear effects are four-wave mixing (FWM), stimulated Raman scattering (SRS), and cross-phase modulation (XPM)(13).

Section 1 Four-wave mixing

The nonlinear crosstalk caused by the four-wave mixing effect in the WDM system is generated as long as three waves of ω_i, ω_j and ω_k propagate simultaneously in the fiber(9), and the four-wave mixing effect can be in a new one. A new light wave is generated at the frequency point $\omega_F = \omega_i + \omega_j - \omega_k$(3). For a system with M channels, i,j,k can vary from 1 to

M, and each group corresponds to a new frequency. Point, this produces a lot of new frequency points. When the channel spacing is equal, most of the new frequencies are the same as the original channel frequencies, and coherently interfere with the original signals in the channel. When the channel spacing is not equal, most of the new frequencies fall between the original frequencies, forming noise. Whether it is equal channel spacing or unequal channel spacing, the channel power is lost, which in turn affects system performance. However, due to the coherent nature of crosstalk, when the channel spacing is equal, the situation is much more serious.

When the channel spacing is equal, most of the FWM components will fall within the channel spectrum and cannot be clearly observed. However, when these FWM components interfere coherently with the signal, they are easily seen in the time domain.

In WDM systems, the need for capacity expansion forces people to maximize spectrum utilization, which makes the channel spacing of the system more and more dense, and the crosstalk caused by the four-wave mixing effect becomes severe, so the four waves are controlled. The influence of the mixing effect is of great significance.

In general, there are several ways to reduce the effects of the four-wave mixing effect(2).

(1) Adopt a suitable dispersion management scheme. FWM efficiency is

closely related to fiber dispersion. The dispersion of the fiber can make the optical signals of the interacting channels have different group velocities, which can destroy the phase matching condition and reduce the four-wave mixing efficiency(3), so increase the dispersion and increase of the fiber. Channel spacing can reduce four-wave mixing crosstalk. Dispersion management refers to the installation of fibers with different dispersion on the fiber link, and to ensure that the total dispersion value of the fiber is zero, which not only suppresses the four-wave mixing crosstalk, but also eliminates the limitation of the fiber dispersion on the transmission distance of the system.

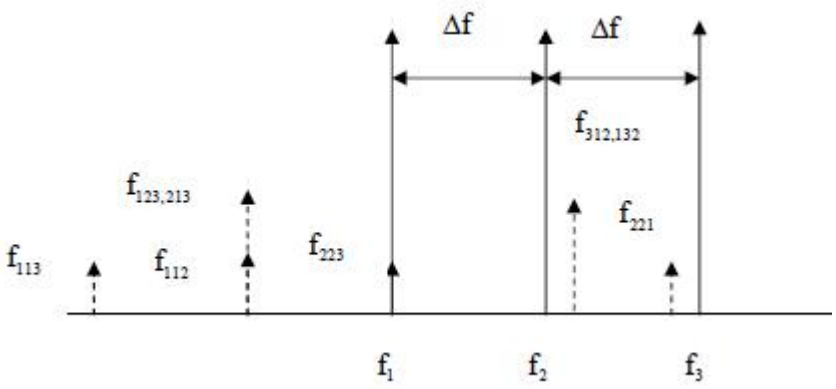

Figure 2.1 New frequency generated by FWM when channel spacing is equal

(2) Adopt unequal spacing channel configuration. When the channel spacing of the system is equal, the newly generated frequency of the FWM falls on the channel. At this time, the FWM crosstalk in the fiber is the most serious, and the unequal-space channel configuration can make the new frequency point generated by the four-wave mixing fall at all.

Outside the channel, as shown in Figure 2.1. The unequality of the channel spacing is not arbitrarily chosen, and it is necessary to meet the relevant recommendations of the ITU-T (International Telecommunication Union Telecommunication Standardization Organization) that the channel spacing must be an integer multiple of 100 GHz(17). This approach comes at the cost of occupying a huge bandwidth of the system and requires a new multiplexer to work with.

(3) Utilizing polarization multiplexing between adjacent channels. Constant changes in the polarization state between adjacent channels can destroy phase matching conditions, thereby reducing the generation of four-wave mixing effects.

Section 2 Stimulated Raman scattering

Stimulated Raman scattering (SRS) is caused by the interaction of the light field with the photons (8), during which the medium exchanges energy with the photons. When the incident photon (ie, pump light) enters the fiber, the photon transfers a part of the energy to the photon, causing its molecular vibrational dynamics to transition from a low energy state to a high energy state(16), and the photon frequency is correspondingly reduced, that is, the Stoke frequency shift. Therefore, stimulated Raman scattering in an optical fiber can produce photons of lower frequency, or can provide optical gain to a lower frequency optical field. The cost of

generating a new frequency or providing an optical gain is the consumption of pump optical power.

The generation of stimulated Raman scattering is conditional and can only occur when the pump light exceeds a certain threshold. We can roughly estimate the threshold power P_{th}^{R} of the SRS by observing the scattering intensity in the fiber when it is generated. It means that in the fiber of length L, the incident optical power is half lost to the stimulated Raman scattering when measured from the exit end. The power of light, whose expression is:

$$P_{th}^{R} = 16A_{eff} /(g_R L_{eff}) \quad (2\text{-}1)$$

Where L is the effective length of the fiber, A is the effective core area, and R is the Raman gain factor(15).

In a single-channel fiber system, the SRS effect is generally not considered due to its high threshold. In a multichannel WDM system, the stimulated Raman scattering in the fiber has to be viewed squarely(12). The role of the Manchester amplifier is that as long as the wavelength difference of the signals in any two channels falls within the gain bandwidth, the short-wavelength signal will amplify the long-wavelength signal and its power will be reduced accordingly. In a WDM system, the optical signal with the shortest wavelength can act as the pump light of all other wavelengths of optical light to maximize its power loss, while the

optical signal with the longest wavelength is pumped by all other optical signals to make its power gain reach the maximum.

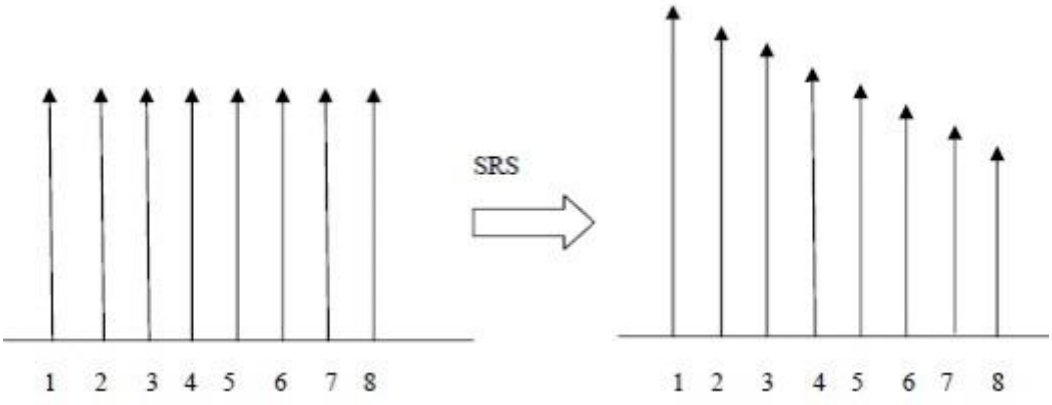

Figure 2.2: Influence of SRS on signal power of WDM channels

Figure 2.2 shows the power variation of each channel's light waves (from low frequency to high frequency) affected by stimulated Raman scattering in an 8-channel WDM system. It can be seen from the figure that the light waves at both ends are most affected. The previous analysis was also verified. This kind of crosstalk originating from the energy transfer between channels is very disadvantageous to the system. It only occurs when the signals of the two channels take the bit "1", which causes the power of the signal to fluctuate, increasing the noise at the receiving end. The system performance is seriously deteriorated.

In order to suppress nonlinear crosstalk caused by stimulated Raman scattering, we have the following methods:

(1) Reduce channel power. Reducing the channel power so that it does not reach the threshold for causing stimulated Raman scattering is the most straightforward method, but it will reduce the system signal-to-noise ratio and has no practical significance.

(2) Using spectrum inversion techniques. Let the stimulated Raman scattering exist on the entire link, and use the spectrum inversion technique to invert the wavelength division multiplexed signal at some appropriate distance, so that the short-wavelength channel and the long-wavelength channel are mutually converted, and finally Raman The direction of the scattered power transfer is reversed, and the power of each channel is approximately equal at the output end of the fiber(20).

(3) Adopt dispersion management technology.

(4) Use large effective area fiber. Large effective area fibers can reduce the core power density and increase the stimulated Raman scattering threshold, thereby improving the system limitation of stimulated Raman scattering(19).

Section 3 Cross phase modulation

In an optical fiber, when the incident light is strong, its refractive index changes with the amplitude of the optical field . When light waves of different frequencies propagate in the optical fiber, the amplitude modulation of each optical wave changes the refractive index of the optical fiber(12), and other optical waves Affected by this change, it is equivalent to nonlinear modulation of light waves. This phenomenon is called cross-phase modulation (XPM). In the intensity modulation-direct detection wavelength division multiplexing system, due to the influence

of cross-phase modulation, the fluctuation of the power of one signal will cause the phase of other signals in the fiber to change(7), and then the modulation of the system tends to be caused by group velocity dispersion (GVD). Unstable, eventually leading to crosstalk between channels. When the number of multiplexed channels in the WDM system is small and the modulation rate of the signal is low, cross-phase modulation has little effect on system performance, but as the number of multiplexed channels increases and the signal modulation rate increases, the effect It will gradually emerge.

Taking a two-channel multiplexed WDM system as an example, the signal wavelengths in the two channels are respectively λ_1 and λ_2, the modulation rates of the two channels are equal, and the effects of fiber dispersion are not considered, that is, the two channels have the same group velocity. Figure 2.3 shows the change in power after the interaction of the two signal pulses. he optical pulse signal with a wavelength of λ_2 generates cross-phase modulation for the optical pulse signal of wavelength λ_1 due to the nonlinear effect of the optical fiber, and generates self-phase modulation (SPM) for itself, causing phase fluctuation, and exhibits the amplitude of optical power at the receiving end. Similarly, the optical pulse signal with a wavelength of λ_2 generates cross-phase modulation for the optical pulse signal with a wavelength of λ_1 due to the nonlinear effect of the optical fiber, and generates self-phase

modulation for itself, causing phase fluctuation and appearing as receiving optical power. The amplitude changes, which leads to the loss of the optical power of the system, which in turn affects the receiver's reception of the signal and limits the performance of the system.

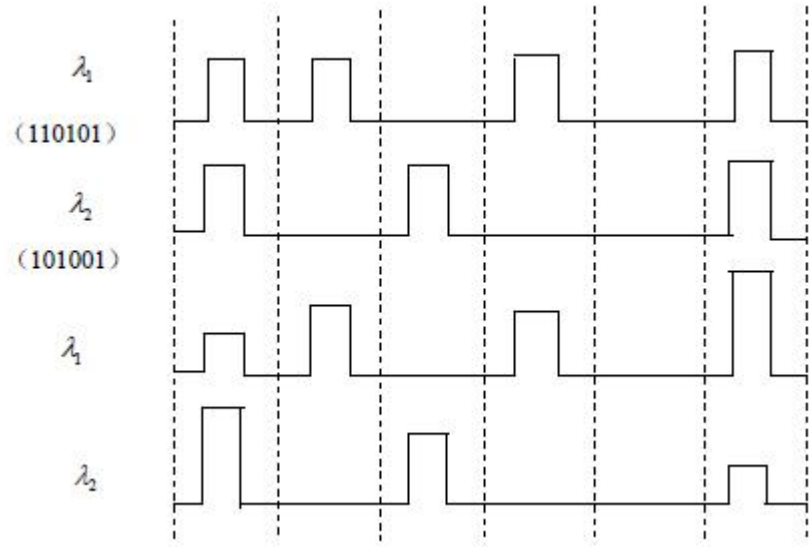

Figure 2.3: Signal pulse interaction power variation in two-channel wavelength division multiplexing system

For crosstalk caused by cross-phase modulation, we can study its suppression method from several aspects:

(1) Increasing the effective area of the fiber used, the effective area in the fiber refers to the average area of the light used to transmit the power of the optical signal, and increasing the effective area of the fiber increases the threshold of the nonlinear effect in the fiber, thereby The system has the ability to transmit more power(2).

(2) Control the maximum channel number, maximum channel power, and minimum channel spacing.

(3) Using a fiber with a certain dispersion to achieve dispersion

management of the system. Dispersion can make optical signals of different wavelengths move away during transmission, thus weakening the influence of cross-phase modulation on system performance. However, fiber dispersion also broadens the time domain of optical pulse signals during propagation, making the system's bit error rate Rising, severely limits the transmission distance of the system. The dispersion management technology can solve this problem very well. Through the dispersion management technology, the optical fiber realizes the alternating positive and negative dispersion values during the transmission process, and ensures that the total dispersion value of the system is zero.

Section 4 Non linear interference noise accumulation

NLI noise PSD $G_{NLI}(f)$ form has been very significant because it is used to evaluate system performance. Particularly, when $G_{NLI}(f)$ is roughly flat across bandwidth within the provided WDM channels, NLI noise is regarded as Gaussian, additive, as well as local white. Therefore, it will significantly ease the computation of system performance.

Within Figure 2.4, $G_{NLI}(f)$ is shown for the case of an $N_s = 20$ spans NY-SMF system, where the retire optical bandwidth $B_{WDM} = 544$ GHz, which corresponds to the 17 NY-WDM channels in 32 GBaud(42). This figure obviously presents NLI noise PSD have been comparatively flat

across the channels, except for outermost noise. In particular, it is almost completely flat on the central passage, which is also the most affected passage.

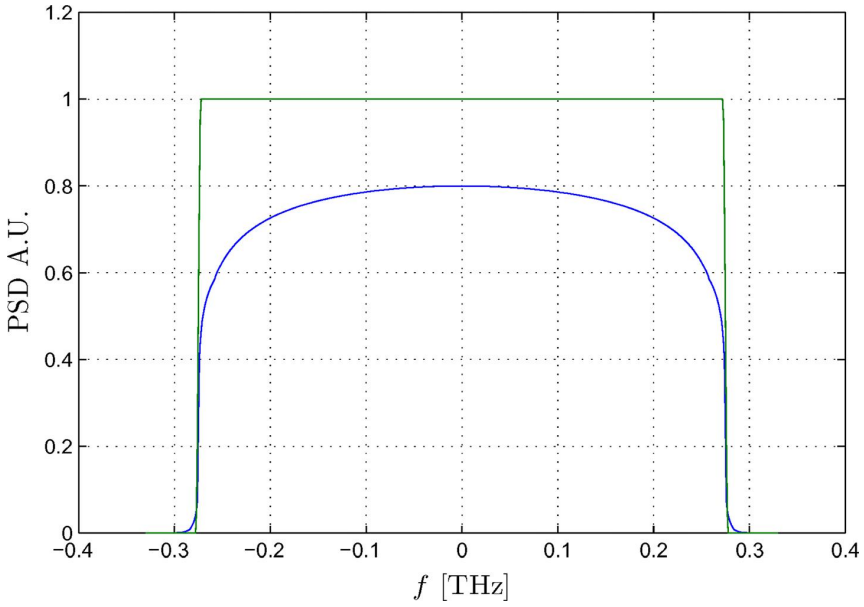

Figure 2.4: Full lines in green: PSD for transmitted signals $G_{WDM}(f)$, equal to seventeen Nyquist-WDM channels in thirty-two GBaud. Full lines in blue: PSD for NLI noises $G_{NLI}(f)$. Within every figure, the signals as well as NLI spectrum is able to adjust the scale freely on easy comparison.(42)

In addition, local white NLI assumes that assumption that values of flat PSD are equivalent to central frequency of the channel are usually cautious about central channels, in other words, result in a bit negative performance evaluation. Within a lot of situation, such a kind of accuracy is really great, or it will be comparatively simple for improving NLI noise variance estimation through assessing NLI PSD within several other frequencies in channels.

A key problem associated with the overall model NLI noise what type of relationship between the cumulative noise generated optical signal bandwidth or channel B, and the number of channel N_{ch}, N_s is the number

of spans. About accumulation and N_s literature now has a variety of experimental results, suggesting that this type of law

$$G_{NLI}(f) = G_{NLI}(f)|_{N_s=1} \bullet N_s^{1+\varepsilon} \quad \text{(2-2)(42)}$$

The estimated value ε between 0 to 0.6. Note, ε= 0 means a span generated in a power sum, i.e. incoherently summed with all other contributions span. Conversely, the ε closer to 1, the greater the correlation between the different spans of NLI, ε=1 corresponds to perfect phase matching(42).

NLI has less reliance channel numbers, which imply that non-insignificant amounts of NLI will be produced though they pass through the channel far from the channel under test.

Accumulation for numerical integration in GNRF obtains the prediction for GN models which caused problem of the NLI accumulation. Process used to derive the results are as follows. G_{NLI} calculates N_{ch}=1 and N_s=1 for each system scenario. In Nyquist-WDM condition, B_{WDM} parameter has been adopted instead of N_{ch}, ranging from one GHz to five THz. Then process resultant information for extracting related data.

A funny part derived according to the next analyses has been that the relationship with the NLI accumulation of bandwidth and distance are not independent, since the relationship between cumulative noise Ns depends on how much light signal bandwidth B_{WDM}.

Subsection 1 NLI accumulation versus Ns

In the Figure 2.5 shows that in the bandwidth is 0.2,1 and 5THz(42), and the fiber is NY-SMF program. The drawn amount has been normalized in the following:

$$g_{NLI}(N_s) = \frac{G_{NLI}(0)|_{N_s}}{G_{NLI}(0)|_{N_s=1}} \quad \text{(2-3)(42)}$$

Qualitative results of NY-PSCF as well as NY-NZDSF are similar. Solid curves have been discovered by GNRF numerical integration. This point is the most suitable. This Figure 2-5 suggests basic index models are very efficient at correctly referring cumulative NLI over entire N_s scope. It will be a significant outcome for it presents one factor ε that has been constant with N_s, entirely characterizes this accumulation.

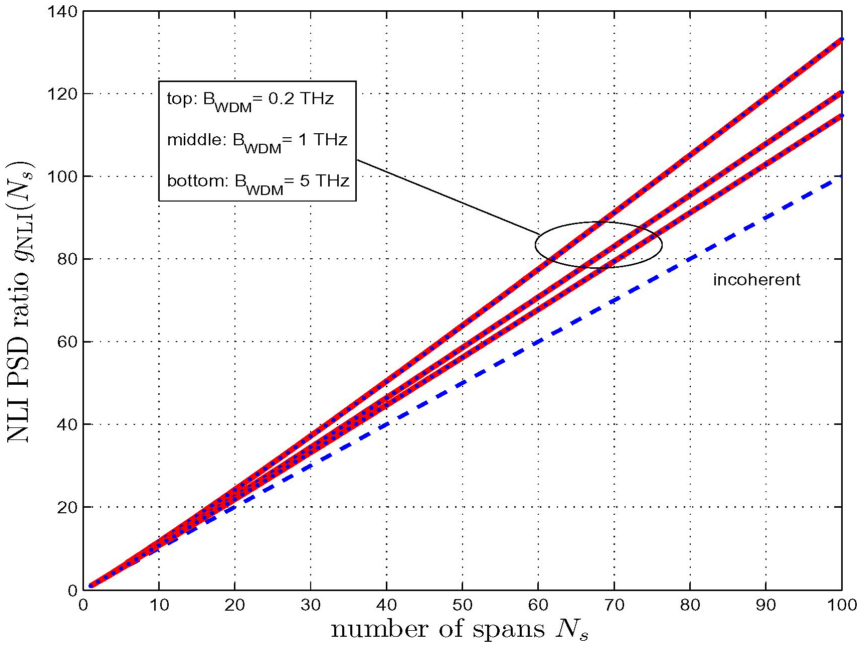

Figure 2.5: Red solid line: $g_{NLI}(N_s)$, regarded to be NLI noise PSD $G_{NLI}(0)$ versus span number N_s, relevant to $G_{NLI}(0)$ and N_s=1, with B_{WDM}=0.2, one and five THz. Superimposed dot in blue: most suitable. Blue dotted lines in the lower part are

inconsistent accumulation to compare.(42)

As the Figure 2.5 shows that the most suitable value of the ε of the NY-PSCF, NY-NZDSF, as well as NY-SMF versus B_{WDM}. And the curves of NY-SMF and NY-PSCF are almost the same. When the Bandwidth is 5THz, all fiber have the same ε which is equal to 0.035. And if the bandwidth of the WDM is 1GHz, all the fiber have the same ε equals to one.

Last values indicate NLI noises generated in one GHz of f equal to zero adds up in the way of phase matching after the span. NLI area increases to N_s, so NLI grows to N_s^2. In contrast, NLI involving a longer frequency will not be a phase match any more with 1 frequency band to next. While B_{WDM} has been higher than 1THz, it is lower than 0.05. It refers to that NLI generally adds up nearly irrelevantly. As a matter of fact, the contribution of NLI occurring having a long distance from f=zero add up within the completely uncorrelated manner because they summarize the other contributions that start in some GHz for f=zero, and these contributions add up in a coherent fashion, so in general It is the weighted average of these different systems that tend to be the same in quantity and tend to zero.

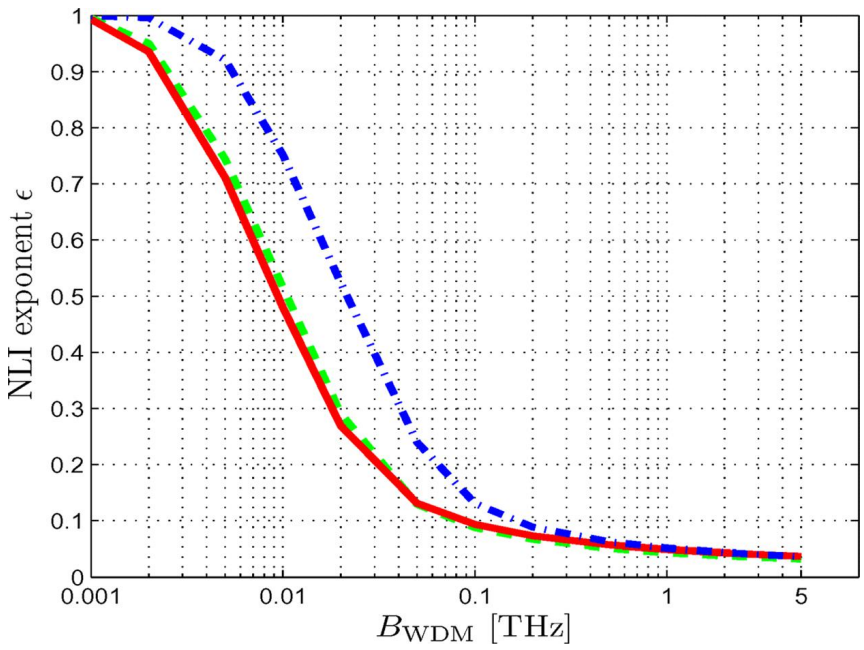

Figure 2.6 NLI cumulative index ε, VS. optical signal bandwidth B_{WDM}, having signals of Nyquist-WDM . Full lines in red: system of NY-LPSCF; dotted lines in green: system of NY-SMF; dotted- dash lines in blue: system of NY-NZDSF .(42)

For non-Nyquist cases, the best fit results from the exponential are as accurate and valid as Nyquist-WDM cases (not shown for simplicity). Figure 2.7 presents the most suitable value of RS-SMF, RS-LPSCF as well as RS-NZDSF with N_{ch}(42). Similarly, this figure presents a qualitatively identical curve, for nearly identical SMF as well as LPSCF. End values are higher than Nyquist, ε= 0.06 for SMF and LPSCF, and NZDSF is about 0.07. The slightly higher e value will be briefly interpreted as shown in the following. SCI contributions referring to N_{ch} equal to one is comparative big: SMF will be 0.19 and NZDSF will be 0.36. Spectra left are basically non-coherently accumulated, but less integral than Nyquist-WDM due to the free guard band between the channels. Therefore, entire Nyquist WDM situation has been a bit larger.

If channel interval is increased f=100GHz, is consistent with the explanation given above, the value tends to increase further. The value in 51-channels (entire C band) will be: RS-SMF is 0.09; RS-LPSCF is 0.096; RS-NZDSF is 0.123. If the span length Ls instead reduced to 50km, while maintaining f = 50GHz and N_{ch} = 100, the RS-SMF is 0.088; RS-LPSCF is 0.090; RS-NZDSF is 0.103. In other words, for C-band systems, significantly increase channel interval and reduce the length of span will result in the great growth, but still comparative small in C-band system.

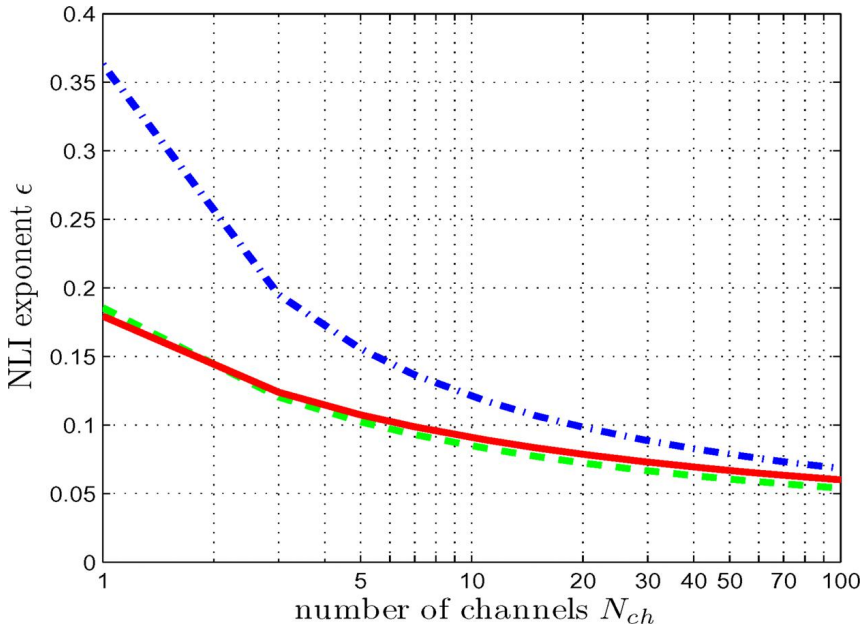

Figure 2.7: NLI cumulative index ε, VS. channel number N_{ch}. Full lines in red: system of RS-LPSCF; Dotted lines in green: system of RS-SMF ; Dotted -dash lines in blue: system of RS-NZDSF.(42)

Subsection 2 NLI accumulation versus B_{WDM}

As the Figure 2.8 shows the non linear interference cumulative noise versus optical signal bandwidth in the NY-SMF, function (2-4) is as follows:

$$g_{NLI}(B_{WDM}) = \frac{G_{NLI}(0)|_{B_{WDM}}}{G_{NLI}(0)|_{B_{WDM}=5THz}} \quad (2\text{-}4)(42)$$

In the N_s=1, 10, 50, the curve is like the logarithmic law. The standardization of g_{NLI} allows direct reading of the bandwidth corresponding to all parts of total C-band noises. Such as, with respect to produce N_s = 50, 50% of the graph shows the noise spectrum only the signal generated before 200GHz, this also means that the remaining 50% of the signal spectrum outside 4.8THz(42).

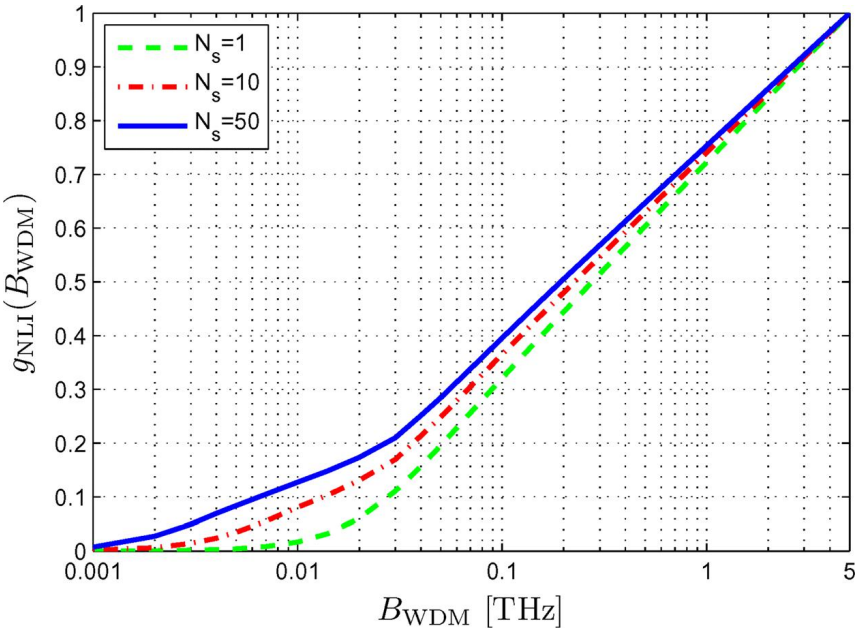

Figure 2.8: Plot of $g_{NLI}(B_{WDM})$, regarded to be NLI noise PSD $G_{NLI}(0)$ VS. B_{WDM}, relevent to $G_{NLI}(0)$ in B_{WDM}=5THz, to the system of NY-SMF. Within the figure, N_s is span number.(42)

When N_s is large, the low bandwidth causes more NLI noise as they have a higher frequency as previously described, so their contributions to NLI are boosted by larger N_s. This fact leads to 50% of the bandwidth is moved to cross a lower value to increase N_s.

As the Figure 2.9 in the RS-SMF we can have a function (2-5) of the

N_{ch}:

$$g_{NLI}(N_{ch}) = \frac{G_{NLI}(0)|_{N_{ch}}}{G_{NLI}(0)|_{N_{ch}=101}} \quad (2\text{-}5)(42)$$

The three different curves, N_s equal to one, ten together with fifty. Now, NLI noise also increases logarithmically based on the logarithmic law, without saturation signs. Similarly, g_{NLI} lets direct reading of the number of channels that produce a total C-band noise portion. Such as , fifty percent of the noises will be generated through first channels of three, five together with six, and N_s are fifty, ten, one separately. The comments are identical to the one in the case of Nyquist-WDM, which you are able to do now about curve-level comparisons.

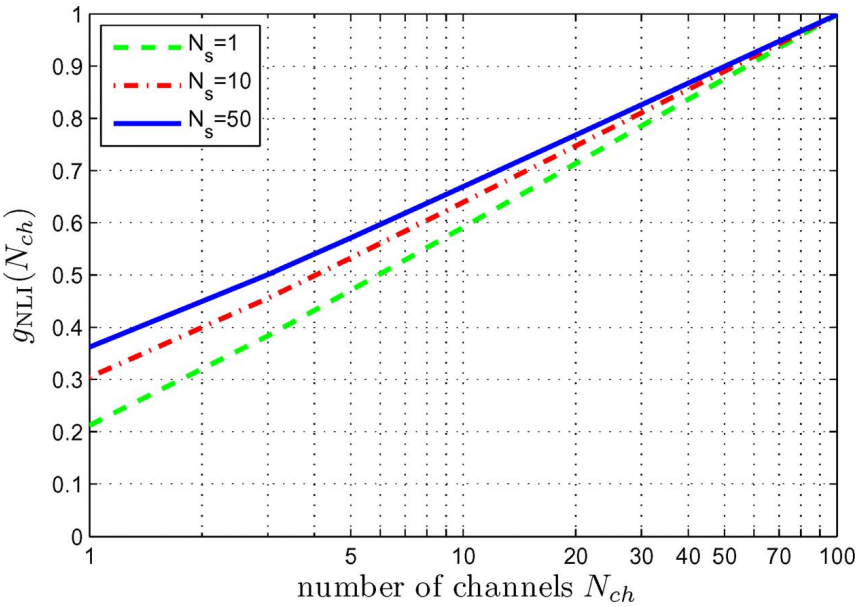

Figure 2.9: Plot of $g_{NLI}(N_{ch})$, regarded to be NLI noise PSD $G_{NLI}(0)$ versus channel number N_{ch}, relevant to $G_{NLI}(0)$ in N_{ch}=101, to the system of RS-SMF. Within the figure, N_s has been span number.(42)

Subsection 3 Conclusion of NLI accumulation

Due to space constraints, the former outcomes can just explore a restricted number of scenes. But we are able to draw some conclusions about the accumulation of NLI GN model predictions.

First of all, by the simple exponential gives the NLI seems sufficient to represent the relationship between growth and N_s of a specific system scenes.

Second, while considering the completed filled systems of standard 50 GHz spacing, ie. spanning the entire C-band or larger, NLI accumulation approaches N_s linearly, ie. Noises add up to in large part incoherently. Residual index is typically about 0.06 and is nearly independent to fiber type used. Pay attention to that if channel number will be small, particularly if the interval is relatively large, you can see that the actual ε is larger.

The recent simulation results and the partially reported experimental results appear to be consistent with the prediction of NLI accumulation and N_s. However, it has to be pointed out that the e values reported by other people is larger than the e forecast with GN models. Obviously, greater studies and cautious comparisons for analytical, simulation as well as evidence in the experiment are even the required conditions for solving this problem.

Third, NLI noises may generate from far-flung channel, while

virtually no enough channels are negligible. In particular, XCI will be in charge of the continuous increase in NLI.

This last aspect can have important implications if further experiments are confirmed. Specifically, twelve together with thirteen, which is understood to be the NLI noise fractional number, can be made up with receiver in theory. Its optical bandwidth refers to x-coordinate as long as receiver has been configured with a non-perfect Digital Signal Processing (DSP) nonlinear compensation algorithm.

For example: Figure 2.9 shows that in a 50-span RS-SMF case, fifty percent of NLI noises in the central channels are generated through the central channels as well as the 2 neighbouring channels (a total of 3 channels). It refers to means for reducing P_{NLI} in central channels with fifty percent(3dB), receiver will require a sufficiently wide optical bandwidth for making sure that these 3 channels are fully visible (approximately 132 GHz) at the same time. Unfortunately, as shown in Section 12B, P_{NLI} has a 3dB increase in system length by only 1dB (25%). For greater benefit, according to Figure 2.9, requires a daunting large receiver bandwidth and associated DSP processing power. The outcomes show electronic nonlinear mitigation can come across actual obstacles to implement with great challenges.

Chapter 3 Non linear interference in frequency domain model

Section 1 Frequency domain model

In these few years, there are many models used UT in the nonlinear propagation. We can classified them into three kinds of models: model of Volterra-series(VS), model similar to four-wave-mixing(FWM) and model of GN.

Volterra-series can be separated in two kinds of domain, one is frequency and another is time domain. At first, we talk about the frequency domain VS. and next section we will talk about the time domain VS. In the dispersion optical fiber, Volterra series method usually use nonlinear Schrödinger equation (NLSE) to get the analytical solution. Because it is difficult to get an exact solution for the general NLSE, so we just think about the first order of Volterra-series expansion, as (3-1) and (3-2).

$$\frac{\partial A(z,t)}{\partial z} = \hat{D}\, A(z,t) + i\gamma \mid A(z,t) \mid^2 A(z,t) \quad \text{(3-1)(30)}$$

$$\hat{D}(z) = -\frac{\alpha}{2} + i\frac{\beta}{2}\frac{\partial^2}{\partial t^2} \quad \text{(3-2)(30)}$$

FWM-like models are separated by the signal spectrum, and put the spectrum into spectral components. Now it usually deal with the OFDM

coherent systems, which each WDM channel will be separated into many electric sub-carrier. Interestingly, the results and the performance of the VS and the FWM-like model are almost similar.

Recently there is another important approach which is based on frequency domain, The model generated by this method is often called the Gaussian Noise model, and many solutions in papers about the influences. This approach give us a assumption that additive Gaussian noise can be very similar as non liner noise.

Section 2 GN model

Subsection 1 Derivation

In this subsection we will show the fundamental results on the relationship among BER, ratios of signal to noise and optical signal to noise. In order to consider the non linear interference, we modified the SNR and OSNR. By modeling the first properly TX signal we proceed towards assessing variance of the non linear interference noise and signaling with the formulas similar to four-wave-mixing(FWM)

A. BER, OSNR as well as SNR

In the linear transmission, the noise of ASE can be calculated as a function (3-3), SNR has been assessed over the diagram of constellation scattering in the deciding phase of receiver.

$$BER = \psi(SNR) \quad (3\text{-}3)$$

The Ψ depends on the modulation format. For example, the BER of the PM-QPSK is as (3-4).

$$BER = \frac{1}{2} \bullet erfc(\sqrt{SNR/2}) \quad (3\text{-}4)$$

For the other formats (3-5), the SNR is found as

$$SNR = \frac{\overline{A}^2}{\sigma_{ASE}^2} \quad (3\text{-}5)$$

The $\overline{A}^2$ is the average signal constellation points squared distance without noise , which is decided by coherent receiver's whole base band scalar transferring function and transmitted waveform. The signal in the transmitter can not be added both ISI or linear crosstalk, the adaptive equalizer $H_{Rx}(f)$ is shaped, so the function (3-6) is like this. And the σ^2_{ASE} is the ASE noise variance.

$$\overline{A^2} = P_{Rx} \bullet R_s^{-1} \int_{-\infty}^{\infty} H_{Rx}(f)|^2 \, df \quad (3\text{-}6)(33)$$

The P_{Rx} is received power per channel and R_s is symbol rate. $H_{Rx}(f)$ is from the DSP adaptive equalizers in the coherent receiver.

And then we should find how to calculate the σ^2_{ASE}, as the function (3-7):

$$\sigma_{ASE}^2 = \int_{-\infty}^{\infty} G_{ASE} \bullet H_{Rx}(f)^2 df \quad (3\text{-}7)(33)$$

G_{ASE} is the power spectrum density (PSD) of dual-polarization ASE on to the receiver(27).

The BER depends on the SNR, and we should calculate the SNR including the NLI noise as the function (3-8):

$$SNR_{NL} = \frac{\overline{A^2}}{\sigma_{ASE}^2 + \sigma_{NLI}^2} \qquad (3\text{-}8)(33)$$

σ^2_{NLI} is similarity as the function (3-9):

$$\sigma_{NLI}^2 = \int_{-\infty}^{\infty} G_{NLI}(f) H_{RX}(f)|^2 \, df \qquad (3\text{-}9)(33)$$

The quantity G^2_{NLI} (f) is the power spectrum density of Non linear interference(33).

$$G_{NLI}(f) = \frac{16}{27}\gamma^2 L_{eff}^2 \cdot$$
$$\int_{-\infty}^{\infty}\int_{-\infty}^{\infty} G_{WDM}(f_1) G_{WDM}(f_2) G_{WDM}(f_1 + f_2 - f) \cdot$$
$$\rho(f_1, f_2, f) \cdot \chi(f_1, f_2, f) df_2 df_1 \qquad (3\text{-}10)(24)$$

The power spectrum density in the function (3-10) is in the end of the link and in this case the spans is identical and the loss is caused by the amplification of optical. GNRF may be physically as descriptions of spectral jitters each thin sheet WDM signal with all other spectral other sheet by FWM process. This is reflected in the GNRF twice the points represent the three "pumps" the frequency (f1, f2, f3=f1+f2-f) of beating normalized FWM efficiency ρ(f1, f2, f3), and creating an interference

signal at frequency f. And the L_{eff} is used to let ρ to 1 as the maximum.

$$\rho(f_1, f_2, f) = \left| \frac{1 - e^{-2\alpha L_s} e^{j4\pi^2 \beta_2 L_s (f_1 - f)(f_2 - f)}}{2\alpha - j4\pi^2 \beta_2 (f_1 - f)(f_2 - f)} \right|^2 \cdot L_{eff}^{-2} \quad (3\text{-}34)(24)$$

Focus on the third frequency f3, f3 is not in the function (3-11). f3=f1+f2-f, which is in the lumped amplification.

The integrand factor:

$$G_{WDM}(f_1) G_{WDM}(f_2) G_{WDM}(f_1 + f_2 - f) \quad (3\text{-}11)(24)$$

It represents the power spectrum density. The finally factor is as the formula (3-12):

$$\chi(f_1, f_2, f) = \frac{\sin^2(2N_s \pi^2 (f_1 - f)(f_2 - f)\beta_2 L_s)}{\sin^2(2\pi^2 (f_1 - f)(f_2 - f)\beta_2 L_s)} \quad (3\text{-}12)(29)$$

This is called phase array factor which takes coherent interference at the receiver in each span.

Using the function of σ^2_{ASE} and $\bar{A}^2$. We can get the function of the OSNR:

$$OSNR = \frac{R_s}{B_n} SNR \quad (3\text{-}13)$$

The B_n is the bandwidth of OSNR. This formula is just used in the matched Rx filter. Otherwise the formula is more complex.

The formula of the non linear OSNR is as follow:

$$OSNR_{NL} = \frac{R_s}{B_n} SNR_{NL} \quad (3\text{-}14)$$

Finally we calculate the OSNR including the ASE and NLI noise,

$$OSNR_{tot} = \frac{P_{ch}}{P_{ASE} + P_{NLI}} \quad (3\text{-}15)$$

The P_{ch} is power of launched, the P_{ASW} and P_{NLI} is the power of ASE and NLI.

Subsection 2 Configuration

In the past few research, many system configurations was used. They are all based on the three types: SMF, NZDSF and PSCF. The parameter of the three types fiber.

Dispersion parameter is β_2 which can be describe as (c refers to light-speed and the λ refers to wavelength of operating):

$$\beta_2 = | D | \cdot \lambda^2 / (2\pi \cdot c) \quad (3\text{-}16)$$

The B_n is always 12.48dB(0.1nm). We usually use an odd number of channels N_{ch} because we need a central channel. So we choose the N_{ch}= 101. The N_{ch} is assumed to the full C-band which is 5THz(32). The symbol rate is 32Gbaud and the roll off is 0.3. So the full channel bandwidth is 41.6GHz. Span length is 100km and channel space is 50GHz.

There are another three systems which assumed the ideal Ny-WDM transmission which means the channel rectangular spectra is perfectly rectangular and the bandwidth is the same as the symbol rate.

Subsection 3 modeling the transmitted signal

We first make key assumptions, combing to a Gaussian random process by each channel and the total WDM signal. Furthermore, we need a signal spectrum composed of spectral lines, because we are using a method analogous to FWM in assessing NLI. Necessary to meet both requirements, but also the use of complicated periodic white Gaussian noise (PWGN) procedure with a suitable spectral shaping way.

The procedure of PWGN cycle is able to be presented by Karhunen-Loève function (3-17) as follows

$$E_{PWGN}(t) = \sqrt{f_0} \sum_{i=-\infty}^{\infty} \xi_i e^{j2\pi i f_0 t} \quad \text{(3-17)(9)}$$

The f_0 equal to $1/T_0$ and it is assumed for having unit variance of the ξ_k's which have been statistically independent complicated Gaussian random variables of the same distribution: The Fourier transform of formula is

$$E_{PWGN}(f) = \sqrt{f_0} \sum_{i=-\infty}^{\infty} \xi_i \delta(f - i f_0) \quad \text{(3-18)(9)}$$

$$G_{PWGN}(f) = f_0 \sum_{i=-\infty}^{\infty} \delta(f - i f_0) \quad \text{(3-19)(9)}$$

In order to obtain a desired Gaussian noise transmission from the E_{PWGN} (GN) to EGN signal model, we performed spectral shaping of the latter, so that the spectral lines in the final EGN "envelope" the WDM

optical signal emitted from the actual PSD $G_{Tx}(f)$

$$E_{GN}(f) = \sqrt{G_{Tx}(f)}\sqrt{f_0}\sum_{i=-\infty}^{\infty}\xi_i\delta(f - if_0) \quad (3\text{-}20)(9)$$

$$G_{GN}(f) = G_{Tx}(f)f_0\sum_{i=-\infty}^{\infty}\delta(f - if_0) \quad (3\text{-}21)(9)$$

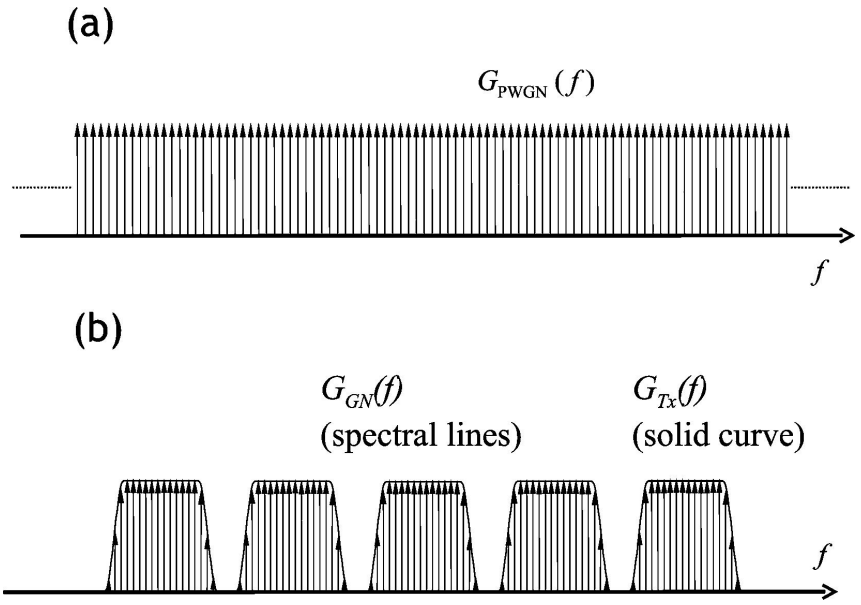

Figure 3.1: (a) PWGN noise's Average power spectrum; (b) Average power spectrum of periodic Gaussian noise with spectral shape(9)

Please note, assuming it is important independent that each frequency component of all other frequency components at the statistics, because ξ_k's is independent of the RV. Also note, EGN cyclical hypothesis does not result in an actual general loss, because the cycle T_0 may be selected as large as desired. It can even become infinite.

Section 3 Enhanced GN model

Most restrictions GN model derived from the assumption of a Gaussian signal. Eliminate the assumption seems to be a necessary step.

Briefly, the signal is assumed Gaussian model calculation means considering only the second time transmission signal. Removing Gaussian assumption to consider the fourth timing signal, XPM, and FWM, SPM, and the fourth and sixth timing signals.

In such an extension is XPM contribution to the NLI. In has completed the contribution of FWM and SPM. Then came the follow-up and several related publications EGN model.

EGN model formula is more complicated than GN model. As with GN model, the main objective is to provide EGN model expression $G_{NLI}(f)$ for the NLI PSD. It can be written as function (3-22),

$$G_{NLI}^{EGN}(f) = G_{NLI}^{GN}(f) - G_{NLI}^{corr}(f) \quad (3\text{-}22)(9)$$

correlation which has the influence of signal without Gaussian into user. In this section, we are focusing on the type of NLI which named SCI, XCI and MCI, orderly presentation EGN model formula (3-23). In other words, we will EGN broken down into:

$$G_{NLI}^{EGN}(f) = G_{SCI}^{EGN}(f) + G_{XCI}^{EGN}(f) + G_{MCI}^{EGN}(f) \quad (3\text{-}23)(9)$$

Please note that the right of each item has a GN model section and a correction section, and function (3-24). For example:

$$G_{SCI}(f) = G_{SCI}^{GN}(f) + G_{SCI}^{corr}(f) \quad (3\text{-}24)(9)$$

For the $G^{GN}_{XCI}(f)$ and $G^{GN}_{MCI}(f)$ is similar. We will point out which one is in their definition formula.

In function (3-23) the contribution of this segment of the NLI GN

model is more likely than traditional classification. Before continuing, we review three kinds of NLI type definitions, to facilitate the reader. In (9) can be found based on the equivalent of the actual position of the spectral components of the WDM signal but more formal definition of a set.

The latter intends to render a negative number, model calibration stressed EGN NLI typically reduces the facts. In fact, if it is assumed PM-QAM signal, it will always be lower NLI. Interestingly, if the signal constellation are Gaussian, the $G^{corr}_{NLI}(f) = 0$, i.e. $G^{EGN}_{NLI}(f) = G^{GN}_{NLI}(f)$.

Section 4 Incoherent GN model

In the section 3, every NLI single span generated the coherent interference on the receiver of the GNRF. As discussed above in in Section 3, in the case where a transparent and homogeneous links, such interference is shown as GNRF integrated factor χ.

Here we introduce a surrogate model GN coinciding with each model on a single span, but in this section we ignored the coherent interference between various spans. The model has been named incoherent GN model(referred to as IGN model). Accordingly, the total NLI end linking PSD is:

$$G_{NLI}^{inc}(f) = \sum_{n=1}^{N_s} G_{NLI}^{n}(f) \quad (3\text{-}25)(24)$$

Within n-th span alone, $G^{n}_{NLI}(f)$ is the non linear interference power spectrum density generated, and then propagated to the Rx via the link all

the way. As the function:

$$G_{NLI}^{inc}(f)=\frac{16}{27}\gamma_n^2 L_{eff,n}^2$$
$$\prod_{k=1}^{n-1} e^{6\int_0^{L_{a,k}} g_k(\zeta)d\zeta} e^{-6\alpha_k L_{a,k}} \Gamma_k^3$$
$$\prod_{k=n}^{N_s} e^{2\int_0^{L_{a,k}} g_k(\zeta)d\zeta} e^{-2\alpha_k L_{a,k}} \Gamma_k$$
$$\int_{-\infty}^{\infty}\int_{-\infty}^{\infty} G_{WDM}(f_1)G_{WDM}(f_2)G_{WDM}(f_1+f_2-f)$$
$$\rho_{n_s}(f_1,f_2,f)df_1df_2 \qquad (3\text{-}26)(24)$$

Where in the subscript integer n, k represents an amount related to the span.

Function (3-25)--(3-26) constitutes a broadly-defined inconsistent or GNRF IGNRF. It is assumed with the homogeneous and transparent connection, IGNRF simplified as:

$$G_{NLI}^{inc}(f)=\frac{16}{27}\gamma_n^2 L_{eff,n}^2 N_s \cdot$$
$$\int_{-\infty}^{\infty}\int_{-\infty}^{\infty} G_{WDM}(f_1)G_{WDM}(f_2)G_{WDM}(f_1+f_2-f)$$
$$\rho(f_1,f_2,f)df_1df_2 \qquad (3\text{-}27)(24)$$

Section 5 The performance of the Frequency domain models

In this section, there is a very important thing is we analysis the results with the model predictions that we find in the recently simulate. Because of the NLI noise, noise accumulation is looked to be "incoherent". As that our cumulative data with incoherent noise demonstrate that the simulation is better than using the coherent accumulation.

Subsection 1 The GN model test result

Most of our tests proceed as follows. For each of fiber type in the different frequency spacing, we estimate the NLI models system to simulate by a transmit power per channel function with L_{tot}. For example, in Figure 3.3(a), we can find the group of PM-QPSK curves on the SMF. In Figure 3.3(b), the identical curves of PM-8QAM has been displayed on the PSCF. The numbers have shown our consistent finding throughout the comparison: the solid lines(model) pretty much similar as the markers(simulation results).

Since it would be impractical to show a similar graph of all twelve combinations of format and fiber, we can analysis the results in different ways. The key information in Figure 3.3 is clearly that we want the maximum data of every curve, which means the maximum L achievable

by the system. We estimate L_{max} for all system configurations by simulating and using the model. We then collected all the results, one L_{max} versus net spectral efficiency (SE) per fiber type, as shown in Figure 3.3. The net spectral efficiency is M that is the number of bits carried per symbol (PM-BPSK is 2, PM-QPSK is 4, PM-8QAM is 6 and PM-16QAM is 8) and Rs = 25GBaud is the symbol rate of net Payload. The last one is achieved through minus FEC and protocol overhead from the total symbol rate of 32GBaud, which we assume will reach 28% worldwide. Draw a different curve for each format and for each fiber while changing the channel spacing parameters. In Figure 3.2, the solid line is the model prediction and the mark is the simulation. The label is the value of the frequency interval.

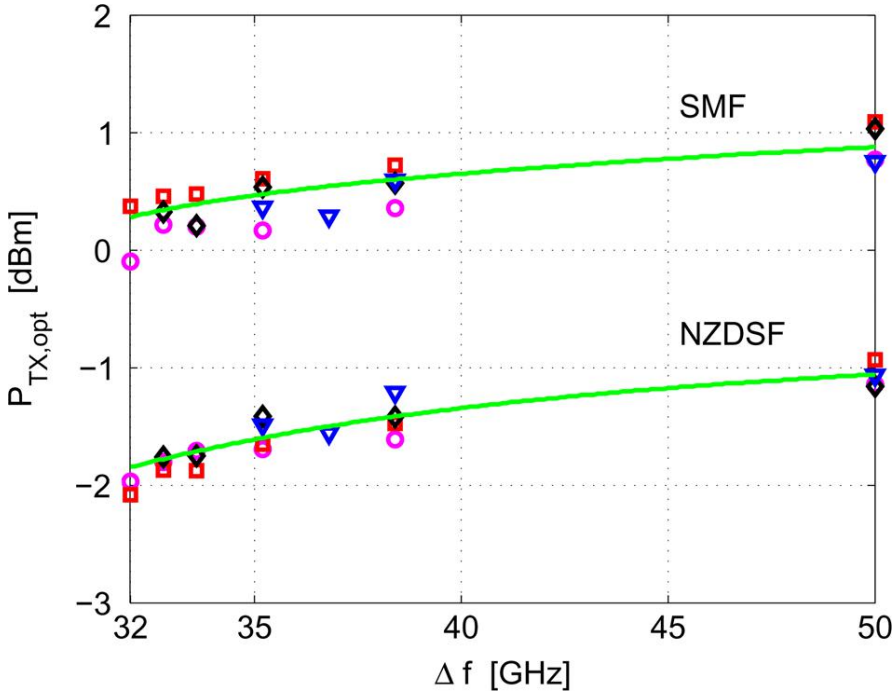

Figure 3.2: optical launch power $P_{Tx,opt}$ being channel interval function Δf for 2 kinds of fibers: SMF together with NZDSF. Full line: predicting models; mark: simulating(circle: PM-BPSK; square: PM-QPSK; diamond:PM-8QAM; triangle:

PM-16QAM) (27).

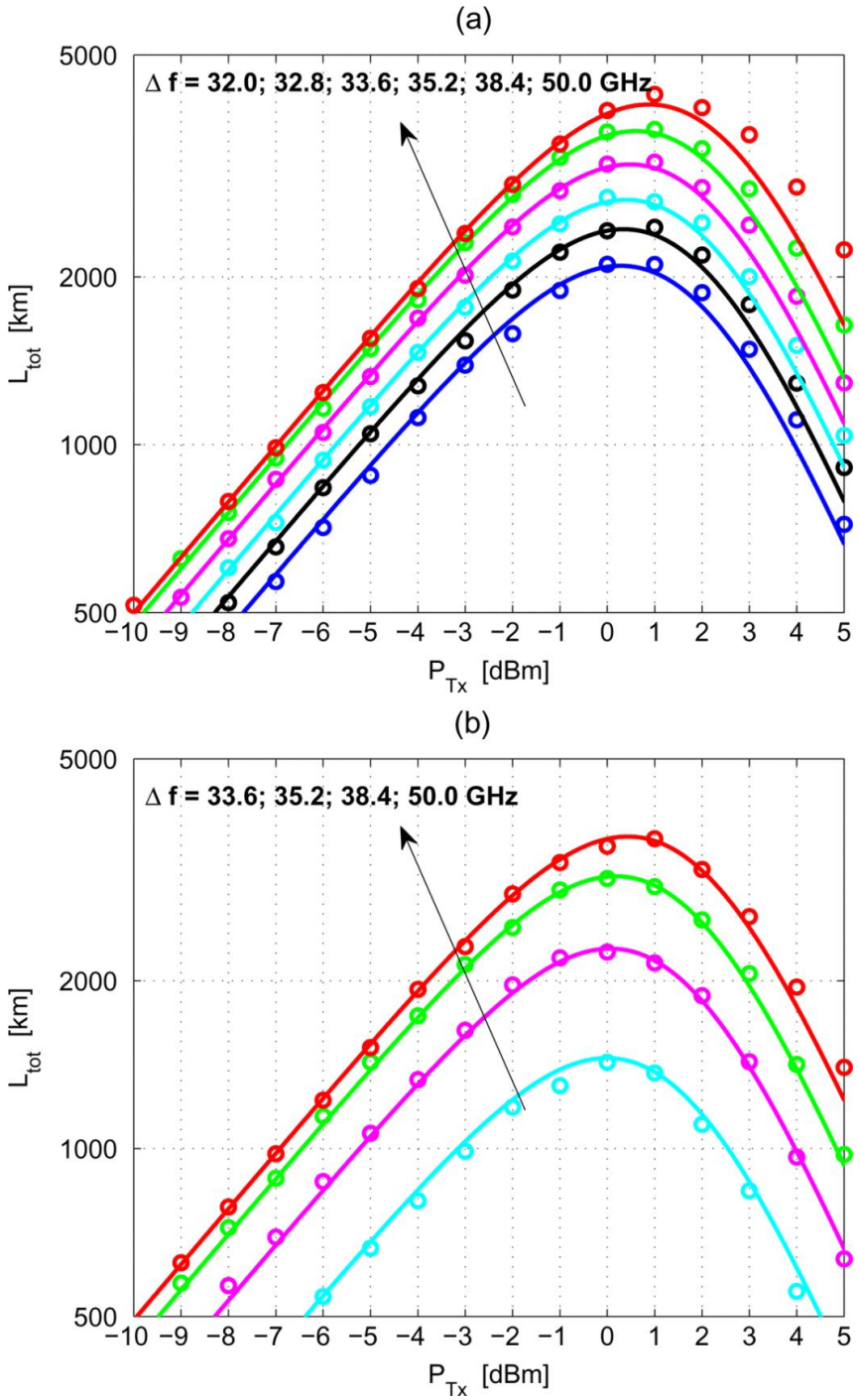

Figure 3.3: The system achieves the relationship between L_{tot} and transmit power per channel P_{Tx}, 9 channels with 32 GBaud, BER=$10^{-3)}$. Full line: predicting the model of GN. Mark: Simulation outcome. Various curves refer to various channel spacing, as shown within the diagram, draw (a) PM-QPSK on SMF; draw(b) PM-8QAM on PSCF (27).

The most striking feature of Figure 3.4 is that two kinds of curves one is model predictions and another is simulations that are excellent in

all modulation formats, fiber optics, and spacing. Note that the distance between these two extremes is very far: from PM-BPSK system in PSCF up to 18000 km and spectral efficiency 1.0bit/s/Hz up to 200km for the PM-16QAM system at a spectral efficiency of NZDSF over 5.7 bit/s/Hz. From this data we can find the model predictive ability is quite extensive.

In addition to the maximum range, another significant parameter for system is the optimal transmit power of each channel(P_{txopt}), ie the transmit power referring to L_{max}. P_{txopt} was collected from all the modulation, fiber as well as spacing. And the relationship between this P_{txopt} and the frequency interval was plotted by us for all formats on the SMF as well as NZDSF fiber as the picture shows within Figure 3.2. The PSCF outcomes have been nearly the same as the SMF results, so do not show in Figure 3.2 because they will overlap the SMF data and we cannot get the curves very clear. Different formats are shown by different type marker. Only two solid lines are model predictions for two type of fiber. Because transmit power per channel versus the frequency spacing is not depended on the model formats. However, the L_{max} is depended on the P_{txopt}, modulation formats and all the parameter, as shown in Figure 3.4. L_{max} will not be the same. Anyhow, these simulation outcomes confirmed the interesting phenomenon.

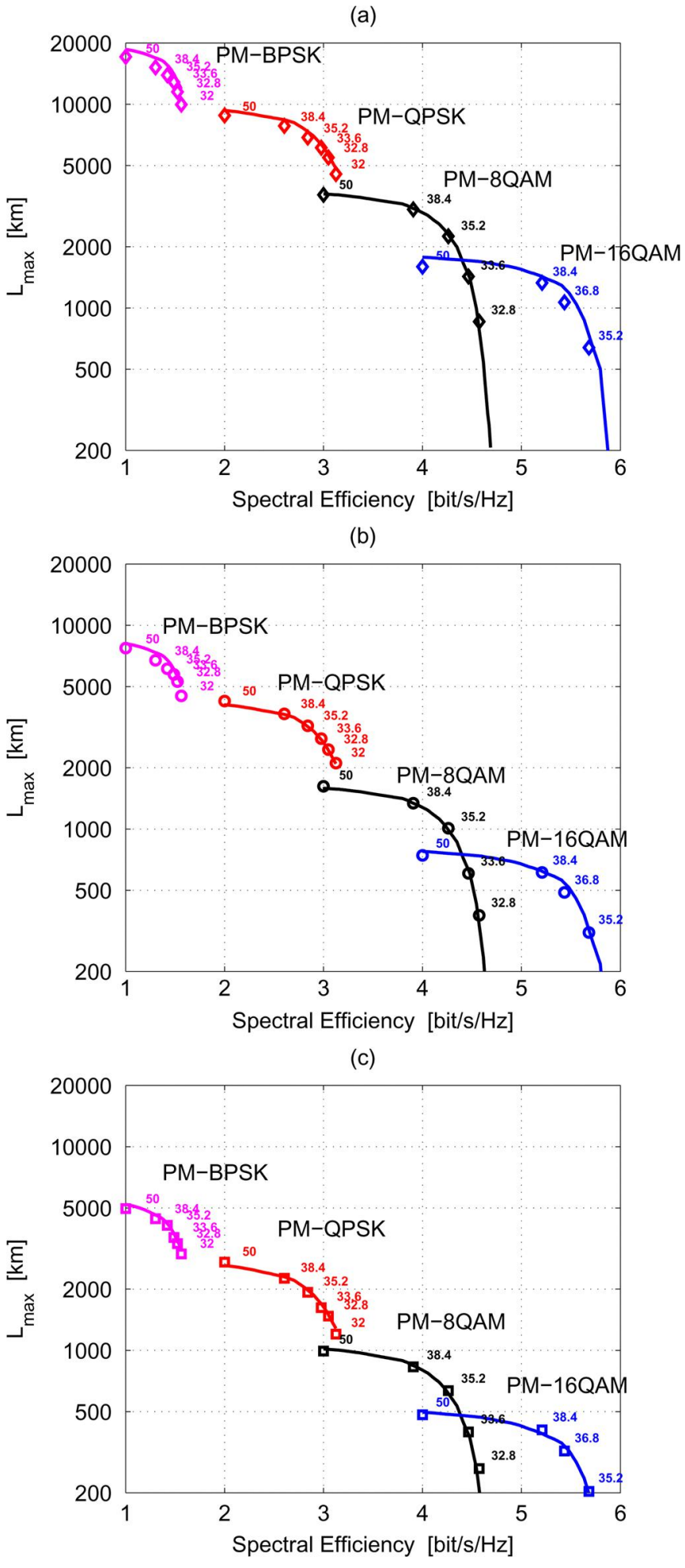
(a)
PM−BPSK
PM−QPSK
PM−8QAM
PM−16QAM
50
38.4
35.2
33.6
32.8
32
36.8
L_{max} [km]
Spectral Efficiency [bit/s/Hz]
20000
10000
5000
2000
1000
500
200
1
2
3
4
5
6
(b)
PM−BPSK
PM−QPSK
PM−8QAM
PM−16QAM
L_{max} [km]
Spectral Efficiency [bit/s/Hz]
(c)
PM−BPSK
PM−QPSK
PM−8QAM
PM−16QAM
L_{max} [km]
Spectral Efficiency [bit/s/Hz]

Figure 3.4: The maximum realizable system achieves the relationship between L_{max} and net spectral efficiency SE, in bits per s / Hz, with 9 channels of 32 GBaud, BER = 10^{-3}. The full line represents the model, while the mark represents the outcome of simulation: every color curve refers to the format in various modulation of the mark in the diagram. The number beside the mark specifies the channel spacing appled within the simulation. a) PSCF diagram. b) SMF diagram. c) NZDSF diagram (25).

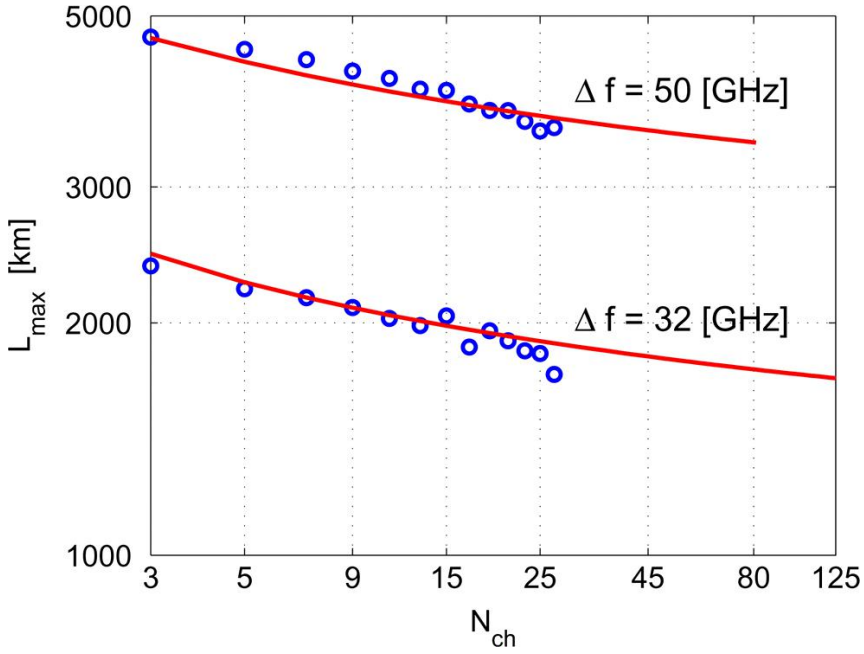

Figure 3.5: maximum achievable system achieves the relationship between L_{max} and the quantity of WDM channels considering the use of PM-QPSK on the SMF at 32 GBaud with channel spacing equivalent to 32 GHz and 50 GHz with BER = 10^{-3}. Full line: predictive model; mark: simulation (25).

In order to further expand the scope of the model test scenario, we decided to increase channel quantity. We specialize in PM-QPSK for SMF at 32 and 50 GHz intervals. The assessed L_{max} and the quantity of transmission channels N_{ch} have been simulated by us. Due to the CPU time limit, we added N_{ch} until it is actually possible. Then, we calculate the model prediction, increase N_{ch} until it is full of the entire C band (4THz), referring to 80 and 125 channels of 50 and 32 GHz, respectively. Result is presented within Figure 3.5, in which the simulation is a marker and the model is solid (25). Even in such a wide bandwidth, the accuracy

of the model can be sufficiently confirmed as long as simulations are possible.

In essence, it can be seen from Figure 3.5 that the performance degradation is not saturated with respect to the number of channels. There seems to be no "adequate" channel in this regard to ensure that NLI is fully considered. However, we can find in Figure 3.5 that performance decreases slowly as N_{ch} increases.

In addition, obviously the performance of several channel experiments doesn't thoroughly represent the performance of the complete system of "C" band. As for this, the model that is shown above may be significantly helpful: Because the models look fairly accurate in predicting system performance and N_{ch}, the performance of several channel systems can be extrapolated through the model so that it can be reliably predicted to be larger the number of channels.

Subsection 2 The incoherent GN model test results

We simulate the incoherent GN-model of the function (3-28) and shown as the figure. In the top Figure 3.6 we used the span length is 100km and in the bottom figure we used the span length is 60km. We use all the 36 and 45 systems configurations of the 'landscape'. The dash line is the results of the simulation. There is a error bar in this results which is 5% (or 10% total).

$$G_{NLI}(f) = N_s \gamma^2 L_{eff}^2 \frac{16}{27} \int_{-\infty}^{\infty} \int_{-\infty}^{\infty} G_{WDM}(f_1) G_{WDM}(f_2) \cdot G_{WDM}(f_1 + f_2 - f)$$
$$\times \left| \frac{1 - e^{-2\alpha L_s} e^{j4\pi^2 \beta_2 L_s (f_1 - f)(f_2 - f)}}{1 - j2\pi^2 \beta_2 \alpha^{-1} (f_1 - f)(f_2 - f)} \right|^2 df_1 df_2 \quad (3\text{-}28)(36)$$

A striking feature is a good model for 500 kilometers accuracy of MR grid line. Even below 500 km, PM-64QAM only exceeded 10% at an MR value of approximately 2 spans (200 km), only with an error of more than 10% on the NZDSF Figure 3.6(top). The GN mode must never dealt with this short-range system, and that the signal should be in the completely dispersed state during most fiber transmissions is the key point. Interestingly, the error size seems to mostly depend on the reach, not the format, the length of the fiber or even the span. With MR over 500 km, the model seems fairly more reliable, independent than any other aspects of the system. Under five hundred kilometers, errors increase gradually, and the model is still in use, which depends on the demand of accuracy.

We should pay attention to that the test within Figure 3.6 does not solve for symbol rates below thirty-two GBaud as well as dispersion below 3.8 ps/(nm*km). That the safety threshold is able to be taken 25 GBaud will be shown in section III. To the dispersion, a lower value below 3.8 ps/(nm*km) has not been proposed by us within this study, namely the NZDSF fiber. It should be conservatively assumed that the GN-Model should not be able to handle near-zero dispersion should not

be close.

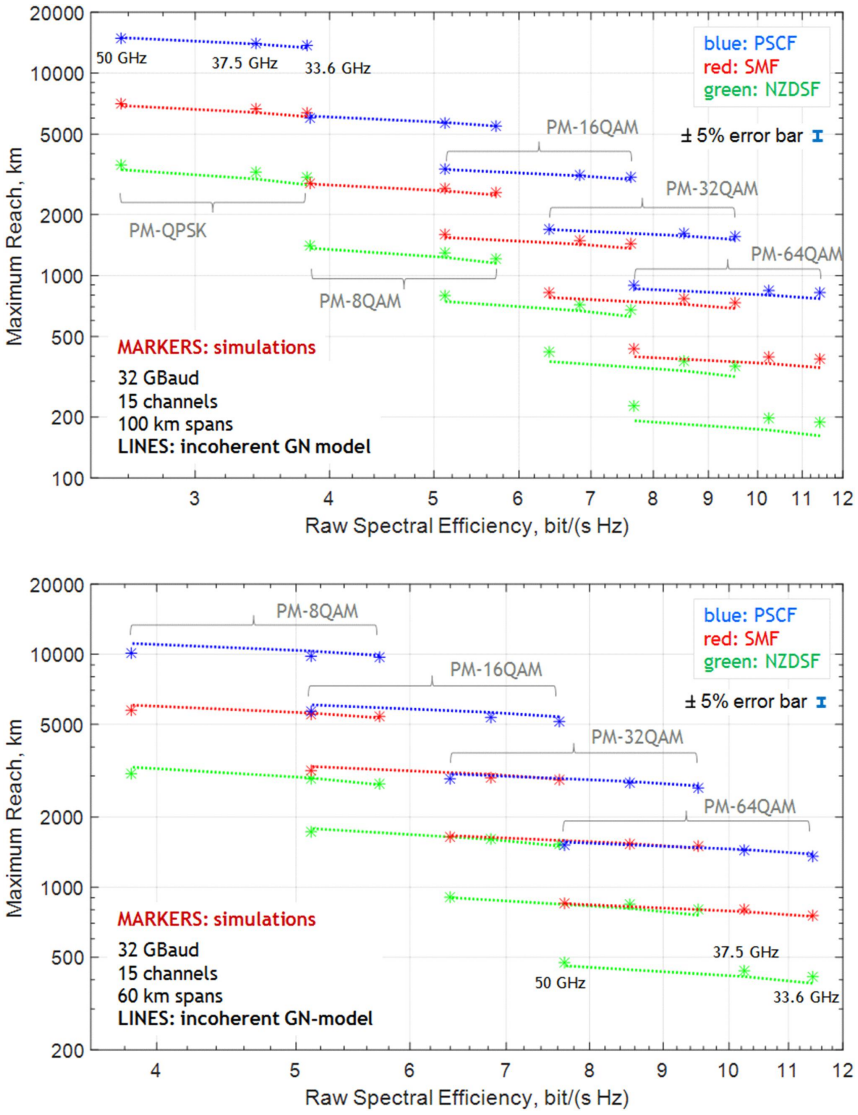

Figure 3.6:

Dashed line: predict maximum reach of the system on the basis of the irrelevant GN model, equation (6-1) and throughout the whole test ‘landscape’, every system is configured with raw spectral efficiency with spans of one hundred kilometers (upper part) and sixty kilometers (lower part), respectively. Mark: Simulation outcomes under 33.6, 37.5, together with 50 GHz channel interval (22).

Subsection 3 Test Outcomes of Closed Irrelevant GN-Model

Although it is very simple, function (3-29) asks for double numerical integration. But assuming the signal of WDM is even, function (3-29) will be solved analytically through a smaller approximation for obtaining

the PNLI closed form as follows :

The solution can be resolved with a smaller approximation to obtain the following closed form of PNLI:

$$P_{NLI} = N_s \frac{16}{27} \frac{\gamma^2 L^2_{eff} P^3_{ch}}{\pi |\beta_2| \alpha R^2} a\sinh(\frac{\pi^2}{2\alpha} |\beta_2| R^2 [N^2_{ch}]^{\frac{R_s}{\Delta f}}) \quad (3\text{-}29)(36)$$

This very simple closed formula reduces the complexity of the model to almost 0. It offers a legible and comprehensible dependency on NLI for parameters of critical system as well. In addition, with these concatenation phases have been approached, it can be imagined that its accuracy may be diminished and therefore needs assessing cautiously.

Figure 3.7 is similar to Figure 3.6, the line now represents MR estimation based on function (3-29). The difference from Figure 3.6 is the smallest among pictures in the 100 km range. In the picture of 60 kilometers range, the error of PSCF situation increases slightly. This has nothing to do with primary functions for the models of GN. It is because of the need for a specific further approximation for obtaining the closed-form settlement to function (3-29). This approximation is valid, as long as the loss of pan will be a little big, the Threshold is approximately ten dB. At a PSCF span with sixty kilometers, the loss will be 10.2 dB, which is why it differs from the numerical integration of Figure 3.6 (bottom). In general, the whole story, including the PSCF, this error is quite inclusive. Considering its simplicity, function (3-29) is valid in

nonlinear modeling of various test landscape systems, MR as well as spectral efficiency are nearly 2 magnitude orders between 2.5 and 11.5 bit / (s·Hz), from our perspectives, is a bit significant.

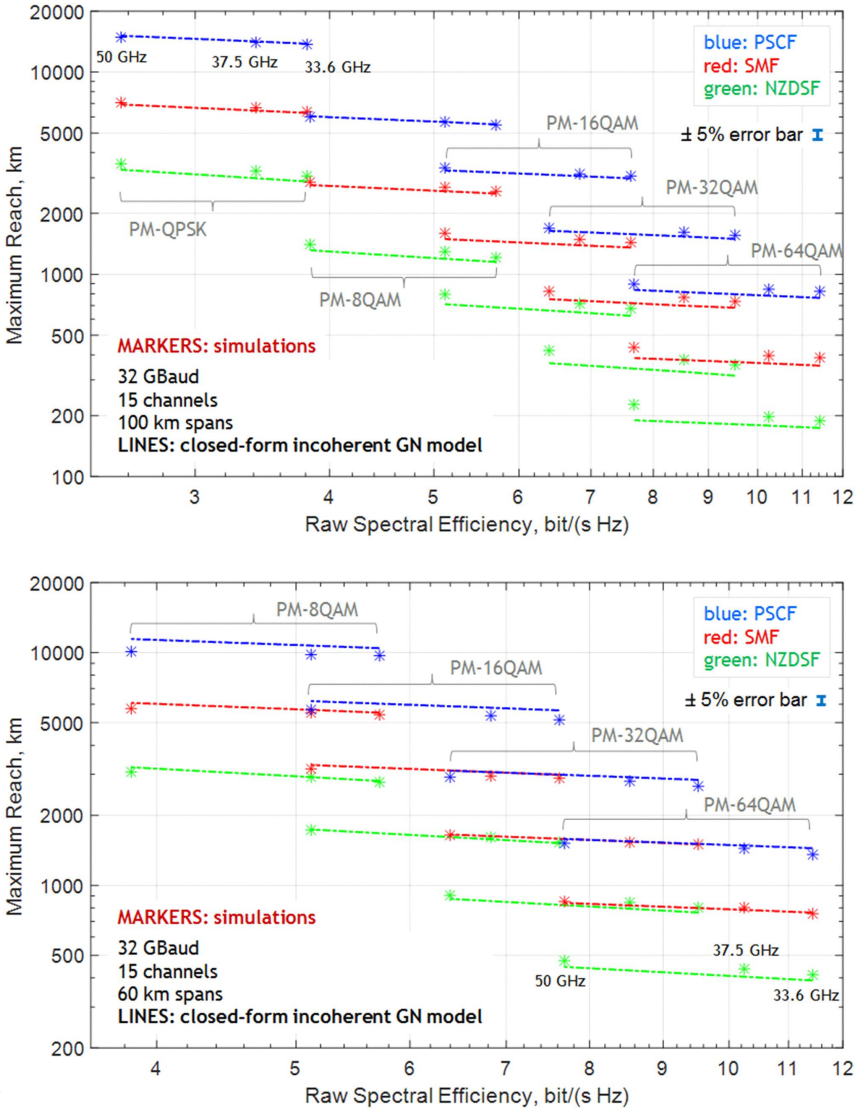

Figure 3.7: Dashed line: predict maximum reach of the system on the basis of the irrelevant GN model, equation (3-29) and throughout the whole test 'landscape', every system is configured with raw spectral efficiency with spans of one hundred kilometers (upper part) and sixty kilometers (lower part), respectively. Mark: Simulation outcomes under 33.6, 37.5, together with 50 GHz channel interval (22).

As mentioned earlier, function (3-29) assumes a uniform, transparent and homogeneous system. All three assumptions can be based on the same type of approximation (3-29) as the derived formula, while still

obtaining the fully closed formula of the incoherent GN model. This general formula offer the quick evaluation means of performance that is of great use for many applications in practice. At present it has applied to the real-time physical layer perceptual controlling plane in the business WDM network of main device vendors(22). This kind of formula can’t be really tested here by us since effective test requires producing a few hundred of uneven together with non-uniform system testing configurations. However, prior to commercial deployment, equipment vendors have conducted extensive experimental testing. However, we ought to keep in mind that the closed formulas take after all limits got in irrelevant GN-model. Additionally, just like what has been described above, the loss of span should be larger than ten dB. In addition, they don’t consider the further.

Subsection 4 Test Outcomes of EGN Model

This test method is similar to IGN model, on the similar "landscape" within the systematic configuration. This result is presented within Figure 3.8. You can immediately see the good corresponding relation in predicting EGN model as well as simulation outcomes in the entire landscape. This agreement has been really compelling because in obtaining two estimated values, calculations between simulation and EGN are quite various within formula as well as algorithm, which is

involving a few trillions of FLOPS. However, the last outcome agreed to be in the range of less than 3%, from 200 kilometers to nearly 16,000 kilometers.

Now we have also achieved very good results in reproducing the more sensitive "P_{NLI}" indicators. Figure 3.7 is similar to Figure 3.8, with EGN estimates added (dashed green line) and non-coherent GN-model curves removed for clarity. A coincidence between 2 and 50 spanning simulation and EGN estimates P_{NLI} which almost perfect equal to 10. More detailed and detailed comparisons between simulation and P_{NLI} EGN estimates can be found, all of which show excellent agreement.

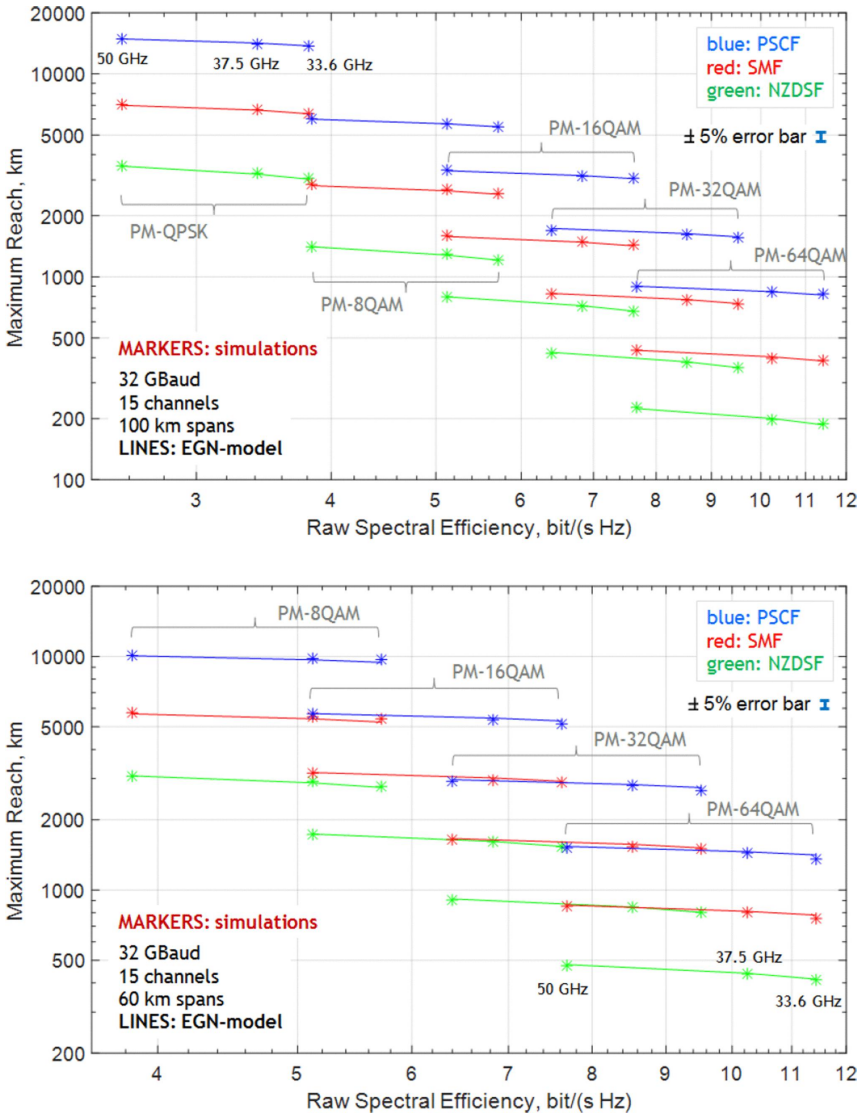

Figure 3.8: Full line: predict maximum reach of the system on the basis of the irrelevant EGN model, and throughout the whole test 'landscape', every system is configured with raw spectral efficiency with spans of one hundred kilometers (upper part) and sixty kilometers (lower part), respectively. Mark: Simulation outcomes under 33.6, 37.5, together with50 GHz channel interval (22).

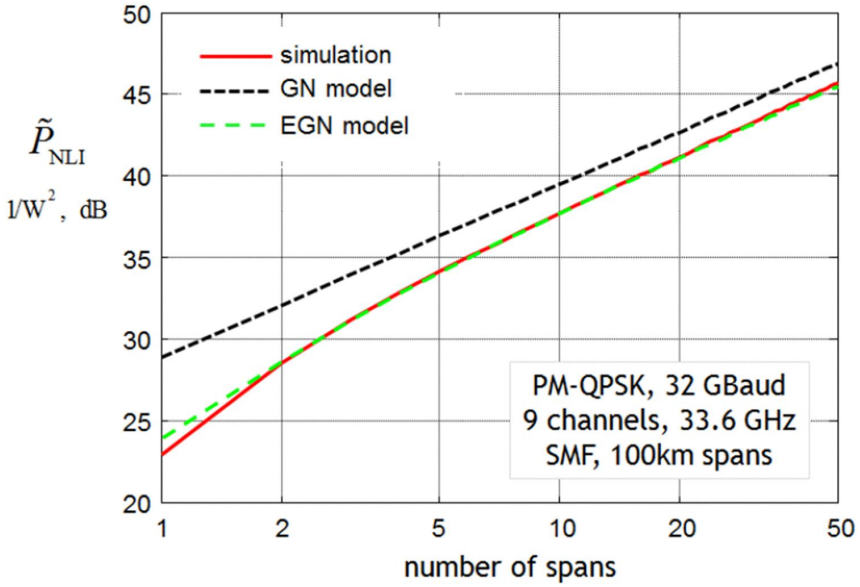

Figure 3.9: The relationship between the cumulative power of the NLI and the span quantity of the incoming link. The normalization of $\bar{P}_{NLI\ ]}$ number VS the transmit power (22).

Subsection 5 Closed Approximation of EGN Model

EGN models' outstanding accuracy, validated within the former parts, has been gained with more analysis as well as computational complexity than GN-model. Therefore, being able to operate it is important for the simple and ideal closed-form approximation. It retains main characteristics of EGN models. It is especially useful for the study of complicated network optimization in which multiple models need to be evaluated to obtain the single outcome.

Within the first phase toward the aim is achieved through determining the closed approximation within corrective item $G^{corr}_{NLI}(f)$, asymptotically effective over the number of spans spanned. However, this approximation does not solve the SPM problem and is limited to a unified

WDM signal. The SPM is taken into account and provides a simpler way that can handle any WDM comb:

$$G_{NLI}^{corr}(f) \approx \underset{\rightarrow}{G}_{NLI}^{corr} = \frac{40}{81}\frac{\gamma^2 P_m N_s L_{eff}^2}{R_m \pi \beta_2 L_s}$$
$$\cdot\left(\sum_{n=1,n\neq m}^{N_{ch}} \Phi_n \frac{P_n^2}{R_n \mid f_n - f_m \mid} + \Phi_m \frac{2P_m^2}{R_m^2}\right) \quad (3\text{-}30)$$

The arrow below G^{corr}_{NLI} reminds approximate asymptotic behavior. The symbols P_n, R_n and f_n correspond to transmit power, sign rate as well as middle frequency for the nth channel. The m^{th} channel has been CUT. Constant Φ_n is decided by the channel's modulation format. Table 1 lists a few major transmit format values.

Format	Φ
PM-BPSK	1
PM-QPSK	1
PM-8QAM	2/3
PM-16QAM	17/25
PM-32QAM	69/100
PM-64QAM	13/21
PM-∞-QAM	3/5
PM-Gaussian	0

Table 1:Values of the φ parameter (22)

Note that G^{corr}_{NLI} isn't decided by frequency. It has been regarded (approximately) constant on frequency band [f_m-R_s / 2, f_m + R_s/2] where f_m will be CUT center frequency, while it will be 0 outside this band. In addition, the homogeneous and crystal connection of aggregated magnification is assumed in the formula. But once the span is different, it may use the average span L_s as well as the effective length $L_{eff.}$ More

approximation applies to all connections with a single span length in ± 15% of mean. Once WDM signal has been consistent and CUT becomes a center channel, it is able to simplify the formula (no more approximation) in the following:

$$\underset{\rightarrow}{G}_{NLI}^{corr} = \frac{80}{81}\Phi\frac{\gamma^2\overline{L}_{eff}^2 P_{ch}^3 N_s}{R^2\Delta f\pi\beta_2 L_s}[HN([N_{ch}-1]/2)+\frac{\Delta f}{R}] \quad (3\text{-}31)$$

where HN represents a harmonic number sequence, it is defined as:

$$HN(N) = \Sigma_{n-1}^{N}(1/n) \quad (3\text{-}32)$$

The plain formula above was tested by us in the ordinary case within system configuration. Our approximate expression (3-33) is:

$$G_{NLI}^{EGN}(f) \approx G_{NLI}^{GN}(f) - \underset{\rightarrow}{G}_{NLI}^{corr} \quad (3\text{-}33)$$

to evaluate the NLI PSD of the CUT, otherwise it was done before. MR results are shown in Figure 3.7. It is worth noting that the accuracy is very good throughout the figure, there is no substantial difference in Figure 3.7. A single exception is the smaller error of PM-64QAM on NZDSF within Figure 3-7(upper part). It is because, like what has been mentioned above, equation (3-33) is asymptotically accurate in terms of the number of spans. Fusion is not fully achieved in MR with only 2 spans.

The results in Figure 3.11 show the possibility of asymptotic approximation to $G^{corr}_{NLI}(f)$. However, an important warning must be mentioned. There are two items to the right of it, which in fact can be

absolute but converse within signs. While 2 quantities are subtracted, the comparative error in outcome may be in excess of the comparative error of the two operands. In particular, we find when contribution of GN model $G^{GN}_{NLI}(f)$ and EGN correction $G^{corr}_{NLI}(f)$ are independent approximations, it may cause great deviation of the right results. We suggest that GN model term $G^{GN}_{NLI}(f)$ is not approximate when using the asymptotic closed approximation of $G^{corr}_{NLI}(f)$, or it uses the very precise fully validated approximation. Especially, taking the place of the $G^{GN}_{NLI}(f)$ together with an approximately non-coherent GN model as talked within previous part is not appropriate. An interesting topic has been left by us, a reliable approximation of the overall closed form as equation(4-21) for investigation in the future. In this part, while approximating equation(4-21) through equation(6-10), we often accurately evaluate the GN model contribution $G^{GN}_{NLI}(f)$.

As shown in Figure 3.11, The question then is whether they remain valid at lower symbol rates. Fig 3.11 presents the relation among a number of channels in which the same number G_{NLI} shown in Figure 3.11 is divided for a given optical bandwidth B_{WDM}. In the figure above, BWDM = 504 GHz, 32GBaud refers to fifteen channels. At the lower part, BWDM = 2.52THz together with 32GBaud corresponds to seventy-five channels. The upper graph presents asymptotic approximation equations which well match the EGN model to about

5GBaud(one hundred channels). The lower diagram presents the slightly inaccurate matching, however, still superior to GN model, or EGN models ignore the FWM. In general, this error is included in the best sign index. It will be 2.4 GBaud or so within these two figures. However, pay attention to that asymptotically approximating curve doesn’t present the min-value, so when performing the optimizing study, you must use the full EGN model.

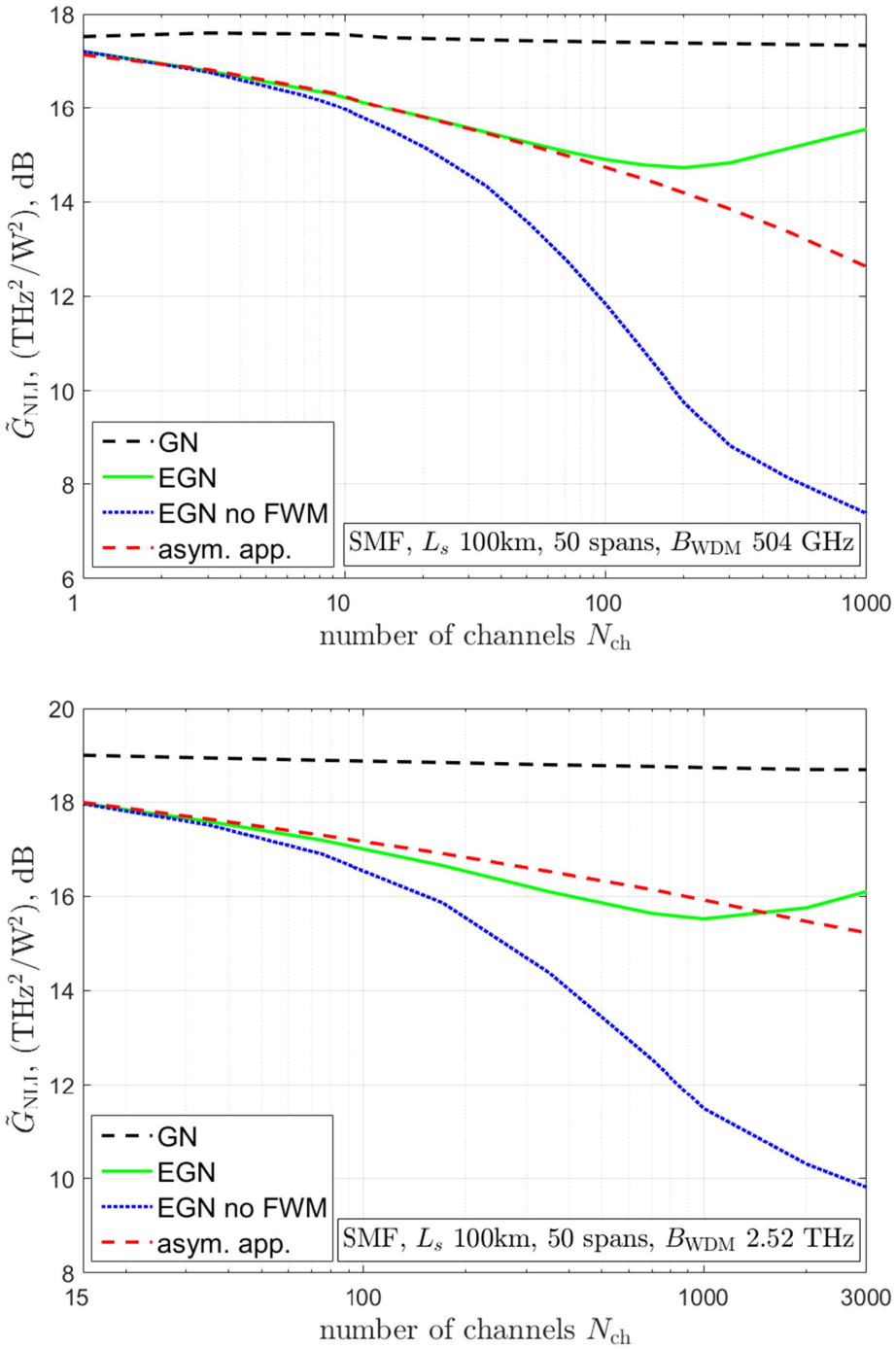

Figure 3.10 Normalized average of NLI noise power spectral density ˜*G* N LI on center channel, vs. channel number *N*ch, for the *fixed* total WDM bandwidth of 504 GHz (upper part) and 2.52 THz (lower part). PM-QPSK modulation, quasi-Nyquist: roll-off 0.05, interval is 1.05 times over the symbol rate. NLI has been measured at 50-span of SMF. Line: Calculation adopting the model shown in the diagram. The tag "asym. app." has been an approximation of the asymptotic EGN model (23).

In summary, closed-form corrections for asymptotic approximations greatly reduce the complexity of the EGN model and are trusty at 32

GBaud or above. To the rate of lower symbols, its accuracy will lose gradually. But it can not be applied to full NLI and research on optimization of symbol rate.

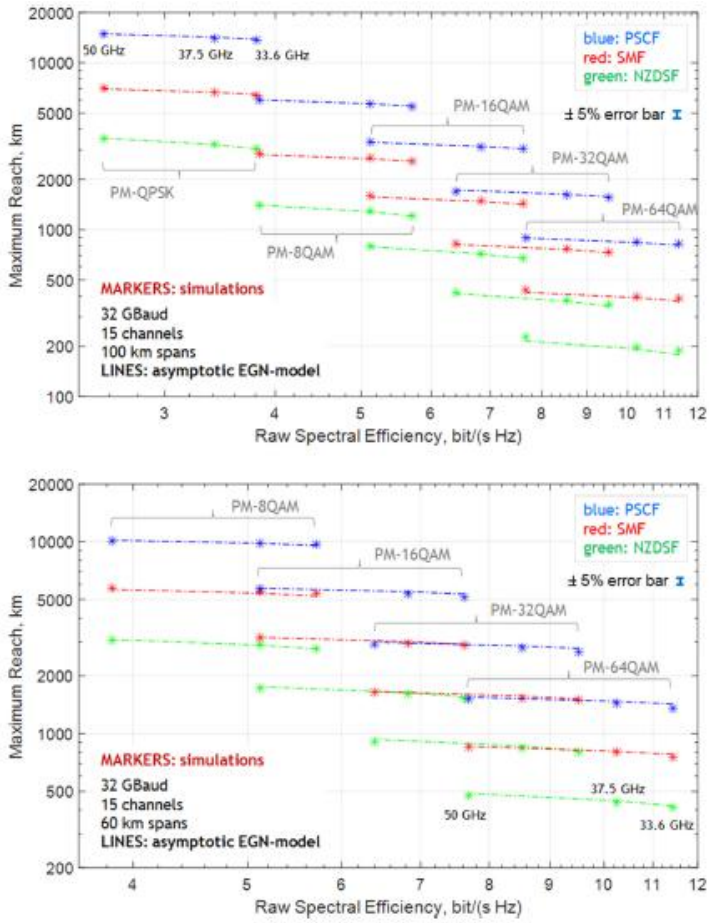

Figure 3.11:Dashed-dotted line: predict maximum reach of the system on the basis of the asymptotic EGN model, and throughout the whole test ‘landscape’, every system is configured with raw spectral efficiency with spans of one hundred kilometers (upper part) and sixty kilometers (lower part), respectively. Mark: Simulation outcomes under 33.6, 37.5, together with 50 GHz channel interval (22).

Chapter 4 Time-Domain Models

Section 1 Time domain model

The another approach is time domain analysis which was covered by Mecozzi together with Essiambre. This approach has been much different from those of former. A larger portion of the NLIN will be seen to be phase noise within non-ignored intensity modulation.The NLIN can be easily canceled out by its long temporal correlation if the NLIN can be characterized as phase noise.

We take an interesting channel in to consideration, setting the center frequency to be 0 freely, while setting the center frequency of the interference channel due to XPM. We involves only interaction with 2 channels, its contribution NLIN plurality of WDM channels are added, there is no need to use more than one pair for initial analysis. We ignore involving the nonlinear interaction of the amplified spontaneous emission noise that in the frame of our ongoing disturbance analysis is negligible. The analysis is possible in principle, but we are here to research conducted found that the first order method with sufficient accuracy. First, we represent our zero-order electric field (linear) settlement:

$$u^{(0)}(z,t)=\sum_k a_k g^{(0)}(z,t-kT)+\sum_k b_k e^{-i\Omega t+i\frac{\beta''\Omega^2}{2}z} g^{(0)}(z,t-kT-\beta''\Omega z) \quad (4\text{-}1)(26)$$

Superscript whole equation represents the "zero-order" (4-1)

represent the right side and the first channel of interest, and represents a second interference channel. Symbol a_k and b_k represent the k-th data symbol from 2 channels carry, z and t have been coordinates of spatial and time, β" has been diffusion factor, T has been the duration of symbol. T_0 simplified symbols, with no generality loss in under the circumstances, β" will be assumed to be negative in this part, Ω is positive. Represents a basic pulse single sign will be g (0)U(z, t) = U(z)g(0, t), in which g (0, t) will be input waveform (21),

$$U(z) = \exp(i\frac{1}{2}\beta''z\partial_t^2) \quad (4\text{-}2)(26)$$

represents the time derivative of the user) with existence of a dispersion propagator.

It is assumed that waveform g(0,t) has been standardized as unit energy and real capacity of transmission symbol being interpreted by the coefficients a_k and b_k (26). Further, assume input waveform g(0, t) is an integer with regarding of the time shift of orthogonal sign duration (26), i.e.

$$\int_{-\infty}^{\infty} g^*(0,t-kT)g(0,t-k'T)dt = \delta_{k.k'} \quad (4\text{-}3)(26)$$

Since the unit of U(z), and this nature has been retained orthogonality linear propagation waveform g (0) (z, t) as well in the.

$u(1)(z, t)$ first order correction of the field has been gained through settling non-linear Schrödinger function (4-4)(26), where zero-order

approximation of the nonlinear term

$$\frac{\partial u^{(1)}(z,t)}{\partial z} = -\frac{i}{2}\beta''\partial_t^2 u^{(1)}(z,t) + i\gamma f(z)\,|u^{(0)}(z,t)|^2\,u^{(0)}(z,t) \quad (4\text{-}4)(26)$$

where g has been nonlinear factor, function f(z) is described along optical link loss/gain profile. In the case of uniformly distributed throughout amplification, is equal to 1, the lumped amplifier f(z) = exp (-az') the case wherein A has been a loss factor, z' has been z position of amplifier's last point. the nonlinear term, leaving only the item of interest help the channel (which is near zero frequency). function (4-5) z = L is direct (26), it is

$$(L,t) = i\gamma\int_0^L dzU(L-z)f(z)\,|u^{(0)}(z,t)|^2\,u^{(0)}(z,t) \quad (4\text{-}5)(26)$$

We are concerned that without loss of generality when detecting the zero symbol data obtained by the reception field of a0, u(L, t) ≃ u(0) (L,t) + u(1)(L,t) by the match filters, the pulse reaction g(0)(L,T) is proportional(26). u(0)(L,t) contribution to the output of matched filter is itself a_0, and u(1)(L,t) is an estimate of the error contribution resulting from Δa_0 NLIN(26). It is given by

$$\Delta a_0 = \int_{-\infty}^{\infty} u^{(1)}(L,t)g^{(0)*}(L,t)dt =$$
$$i\gamma\int_0^L dzf(z)\int_{-\infty}^{\infty} dtg^{(0)}(z,t)\,|u^{(0)}(z,t)|^2\,u^{(0)}(z,t) \quad (4\text{-}6)(26)$$

We have used the definition of linear propagation operator U(L-z)g(0)*(L,t)=g(0)*(z,t)(26). Alternatively zero-order field equations produce a result from the expression (4-1) to (4-6)

$$\Delta a_0 = i\gamma \sum_{h,k,m} (a_h a_k^* a_m S_{h,k,m} + 2a_h b_k^* b_m X_{h,k,m})$$

$$S_{h,k,m} = \int_0^L dzf(z) \int dt g^{(0)^*}(z,t) g^{(0)}(z,t-hT) g^{(0)^*}(z,t-hT) g^{(0)}(z,t-mT) \quad \text{(4-7)(26)}$$

This is the intra-channel interference effects(26),

$$X_{h,k,m} = \int_0^L dzf(z) \int dt g^{(0)*}(z,t) g^{(0)}(z,t-ht)$$
$$\times g^{(0)*}(z,t-kT-\beta''\Omega z) g^{(0)}(z,t-mt-\beta''\Omega z) \quad \text{(4-8)(26)}$$

It accounts for (inter-channel) interference induced XPM(26). Channel interference involves only the symbol transmission channel of interest does not necessarily considered to be noise. It can be reduced by a large block of symbols jointly decoding, may be eliminated by back propagation as well as predistortion. Therefore, the item will be ignored by us with the following formula is proportional to, and will pay attention to NLIN due XPM. Note a provided injection pulse waveform g(0,t), sign duration time T, channel interval parameter W as well as optical fiber, values X_h, k, m will be seen in numbers(26). So as the channels between the discrete, monotonically decreases, which is the ratio between the parameters b"W symbol duration T and the group velocity difference.

$X_{h,\,k,\,m}$ a very important feature is directly proportional to the overlap between it and the four time shifting waveform. Thus, according to the prediction equation it is reasonable. The maximum element $X_{h,\,k,\,m}$ is 0 and h = k = m elements of. This is because in this case, only two shifted waveform need to overlap. We contribute these items written Δa_0:

$$\Delta a_{0_p} = ia_0(2\gamma \sum_m |b_m|^2 X_{0,m,m}) = ia_0\theta \quad (4\text{-}9)(26)$$

We define:

$$\theta = 2\gamma \sum_m |b_m|^2 X_{0,m,m} \quad (4\text{-}10)(26)$$

Note that, since $X_{0,m,m}$ is in accordance with equation , q is a real number, which refers to the non-linear phase and rotation. It is done using subindex p (just like within "phase") within sign inspiration Δa_{0p}. q First two order moments will be provided through the following formula

$$<\theta>= 2\gamma <|b_0|^2> \sum_m X_{0,m,m} \quad (4\text{-}11)(35)$$

$$<\theta^2>= 4\gamma^2 \sum_{m,m'} <|b_m|^2|b_{m'}|^2> X_{0,m,m}X_{0,m',m'} \quad (4\text{-}12)(35)$$

The phase rotation variance will be

$$\Delta\theta^2 = <\theta^2> - <\theta>^2 = 4\gamma^2(<|b_0|^4> - <|b_0|^2>^2)\sum_m X_{0,m,m}^2 \quad (4\text{-}13)(35)$$

Here independence has been applied between the various data signs $<|b_m|^2|b_{m'}|^2>=<|b_m|^2><|b_{m'}|^2>(1-\delta_{m,m'})+<|b_m|^4>\delta_{m,m'}$(31), As their stability $<|b_m|^n>=<|b_0|^n>$. Equation (4-13) constitutes a very important result, i.e., the information symbol phase noise increases with squared amplitude variation and growth, and disappears in the pure phase modulation situation, in which $|b_0|$ will be the constant (therefore $<|b_0|^4>-<|b_0|^4>=0$). In view of the fact that regardless of the modulation scheme by dispersion fiber spread, which is the opposite intuitive result, the electric field intensity appears random fluctuations.

In addition to pure noise after the phase XPM among WDM channels, as well as extra noise contribution, to the single pulse channel of interest of a pair of pulses from the interference channel(21). Since these contributions to residual NLIN, we will NLIN called NLIN, in order to distinguish it from NLIN staging area previously described. Generally, as the left NLIN happens during the time overlaps among 3 or 4 different waveform so amplitude modulation (16QAM, or to be larger QAM constellation) case its amplitude not less than the phase noise, as we used in the digital section 4 as indicated.

Further simplify the phase noise variance limit expression to follow a big cumulative dispersion, and it precisely characterize the case of most up-to-date fiber communication connections aren't included in-line compensation of dispersion. Under this condition, propagation waveform $g^{(0)}(z, t)$ with itself fast Fourier transform is proportional to, i.e.

$$g^{(0)}(z,t) \approx \sqrt{\frac{i}{2\pi\beta'' z}} \exp(-\frac{it^2}{2\beta'' z})\tilde{g}(0,\frac{t}{\beta'' z}) \quad \text{(4-14)(26)}$$

Function (4-14) merely shows the truth that various frequency component of dispersion resulting in the incoming signal travel with various speeds, in order to map the injection signal spectrum to time. Within the above limitation, the factors X_0, m, m is provided through the following formula

$$X_{0,m,m} = \int_{z_0}^{L} dz f(z) \int \frac{d\nu}{4\pi^2 \beta'' z} |\, \tilde{g}(0,\nu)\,|^2 |\, \tilde{g}(0,\nu - \Omega - \frac{mT}{\beta'' z})\,|^2 \quad (4\text{-}15)(26)$$

We define v=t/b"z. In function (4-15) we ignore the non-linear distortion which is produced within the vicinity of input fiber define $z_0 \sim T_2/|\beta''| \ll L$ large as the distance a discrete approximation of Function (4-14) becomes effective use (26). Function (4-15) in the case of fully distributed amplification, we approximate analytical expression of δ_2. Physically, this is equivalent to claiming all collisions in the region of the center $[z_0,L]$ collisions are considered fully collision, despite the fact that some of (those fibers near the edge of the middle collision) part of them are. Will be multiplied by a function of z_m/z (near unity when there are great overlaps among pulses), as well as altering integration order,

$$X_{0,m,m} = \int \frac{d\nu}{2\pi} |\, \tilde{g}(0,\nu)\,|^2 \int_{-\infty}^{\infty} dz \frac{z_m f(z_m)}{2\pi \beta'' z^2} |$$

$$\tilde{g}(0,\nu - \Omega - \frac{mT}{\beta'' z}) \approx \begin{cases} \frac{1}{\beta''\Omega} (0 \le m \le \frac{|\beta''\Omega| L}{T}) \\ 0 (otherwise) \end{cases} \quad (4\text{-}16)(26)$$

The result of the equation:

$$\Delta\theta^2 = (<|\, b_0\,|^4> - <|\, b_0\,|^2>^2) \frac{4\gamma^2 L}{|\, \beta''\Omega\,| T} \quad (4\text{-}17)(26)$$

Simplify the expressions X0,m,m, function (4-17). Also allows to calculate the phase noise $R_\theta(l)=<\theta_n\theta_{n+1}>-<\theta>^2$ time autocorrelation function, notation n is used by us wherein non-linear phase to nth sign within channels of interest induced rotation. Use function (4-18) We

have:

$$R_\theta(l) = 4\gamma^2 \sum_m \sum_n <| b_m |^2 | b_{n+l} |^2 > X_{0,m,m} X^*_{0,n,n}$$

$$- < \theta >^2 = \Delta\theta^2 \left[1 - \frac{| l | T}{| \beta'' \Omega | L} \right]^+ \qquad \text{(4-18)(26)}$$

Wherein [a]+=max{a, 0}(26). In the case where a plurality of WDM channels, function (4-19) is extended to

$$R_\theta(l) = \sum_s \Delta\theta^2(\Omega_s) \left[1 - \frac{| l | T}{| \beta'' \Omega_s | L} \right]^+ \qquad \text{(4-19)(26)}$$

Where W_s has been frequency spacing of the s-th channel as well as WDM channels of interest, then the sum of the interference on channel. Note within the great cumulative dispersion limit, $|\beta'' \Omega_s| L/T >> 1$ characterized in that phase noise of the related long period(26). Such a feature helps use of the available non-linear phase noise cancellation equalization techniques, and helps achieve larger information volume. It helps to extract phase noise in the simulation as well.

Section 2 The time domain model test result

Taking into account the system of 5-channel WDM performed on fiber with standard single mode which dispersion to be seventeen ps/nm/km, non-linear factor γ=1.3[Wkm]$^{-1}$, as well as 0.2dB attenuation per kilometer, the results were obtained from a series of simulations(26). We assume that the Nyquist pulse has a perfect square spectrum with a

32-GSymbols/s sign rate together with 50-GHz channel interval. The simulation sign number per running is 4,096, and the running number per group of system parameters (every system parameter has independent and arbitrary data signs) is from one hundred to five hundred for collecting enough statistical data. The simulations have been carried out using single polarization and theoretical outcomes have discussed scaling in the case of double polarization. For forward-backward circulation, scalar non-linear Schrodinger equation was settled adopting the method of standard split-step Fourier by setting the step size for limiting the largest non-linear phase change into 0.02 degrees(as well as defining 1000 meters within the upper limit). The sample rate is sixteen examples/sign. For extracting NLIN, firstly we remove the average phase shift resulted from adjacent WDM channels and later evaluate the offset receiving constellation point as well as perfect constellation point, which will represent the testing within non-linear case.

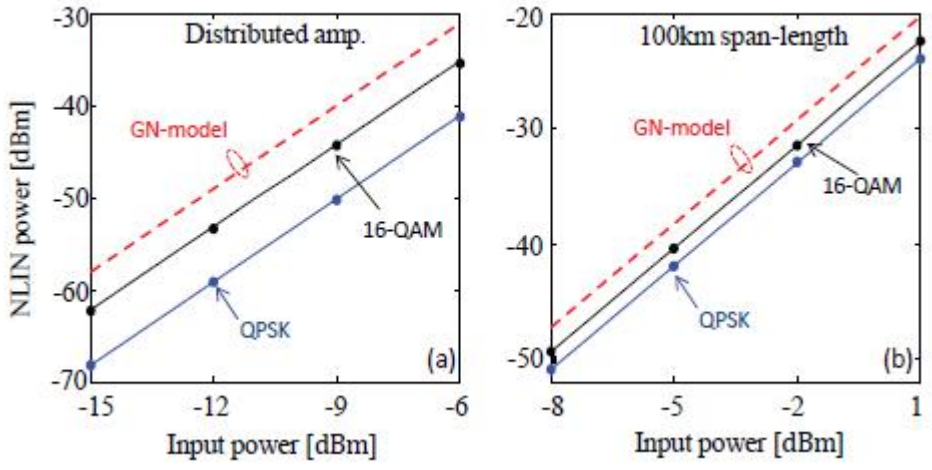

Figure 4.1: NLIN power VS. average power/channel within the 5×100 kilometers

system for QPSK as well as16-QAM modulation. Full line shows theoretical outcomes and dot refers to simulation. Dotted red lines refer to SON contribution P3χ1, and it will be the same to GN model's outcome. (a) Distributed amplification. (b) Aggregated amplification (28).

In Figure 4.1 NLIN power is shown to be the function of average input power of the system by us, which consists of a 5×100 kilometers span in modulation of QPSK and 16-QAM(28). We show the NLIN power as a function of the average input power of the system. In the case of QPSK and 16-QAM modulation, the average input power of the system is 5*100 km(28). Figure 6-12(a) refers to under the condition of pure distribution amplification, while Figure 6-12(b) corresponds to the same system with aggregated amplification. The solid curve and the points show the simulation outcomes. Dotted line in red represents GN prediction model, ie, $P^3\chi_1$. The diagrams show the reliability upon the modulation format, as has been offset of the GN models. But although errors of GN model in QPSK situation are 10 dB to distributed amplification, they are reduced to 3.7 dB while using aggregated amplification. Please pay attention to differences of modulation format and errors in GN model results have nothing to do with input power. The good consistency of theory and simulation will be obvious.

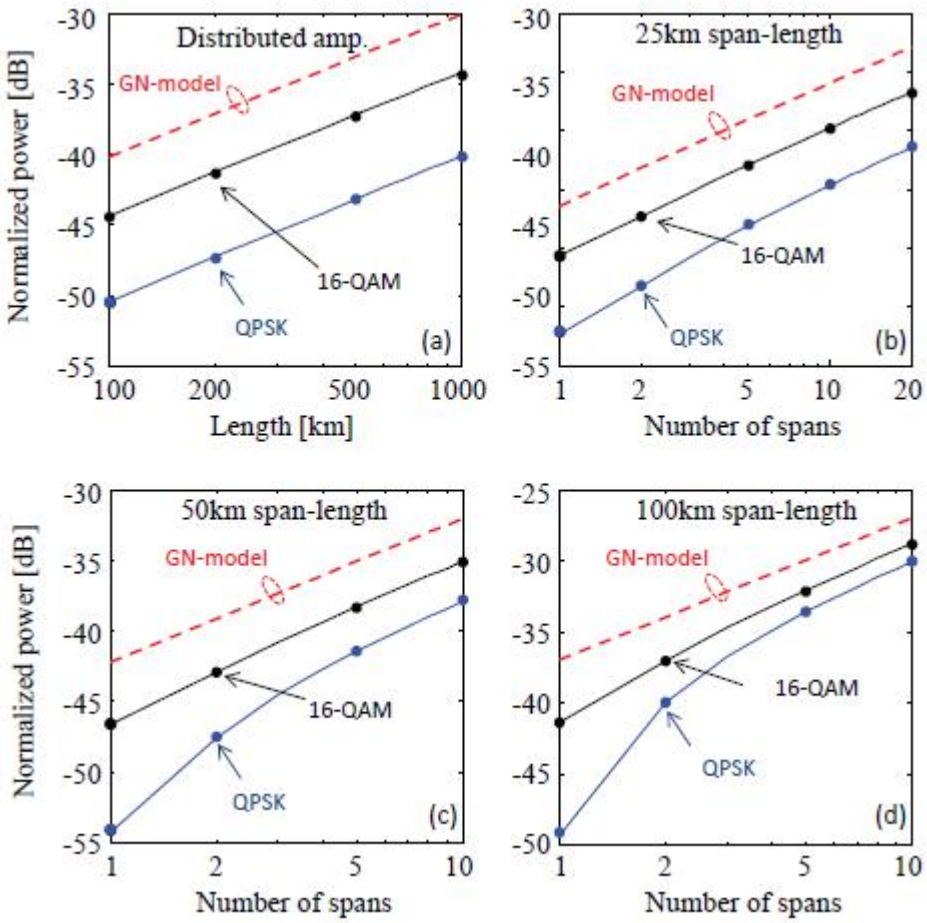

Figure 4.2: NLIN cumulative power (obtained power is normalized) and spans Fig a refers to distributed amplification situation while fig b,c and d refer to the situation of span-lengths with twenty-five kilometers, fifty kilometers, as well as one hundred kilometers, respectively. Full line represent the theoretical outcomes while the dot refers to simulation. Dotted curves in red show SON, or GN model outcome equally (28).

Figure 4.2 suggests NLIN cumulative systems through various lengths of spans. Figure 4.2(a) presents distributed amplification situation , and Figures 4.2(b)-4.2(d) present the case of spans of twenty-five kilometers, fifty kilometers as well as one hundred kilometers, separately. NLIN power within the diagrams has been standardized to the obtained optical power within every situation. Therefore vertical axis is able to be explained to be the ratio of noise to signal. Please note within

single span transmission situation, there is the greatest dependence between modulation format and inaccuracy within GN model. With the increase of span, NLIN goes up faster to QPSK format, while differences among modulation formats decreases. When spreading for 500 km, for distributed amplification, the difference in NLIN power between modulation formats of QPSK and 16-QAM will be about 1.5dB, 2.8dB, 4.8dB, as well as 6dB to spans of twenty-five kilometers, fifty kilometers as well as one hundred kilometers. For distributed amplification, twenty-five kilometers, fifty kilometers as well as one hundred kilometers span cases, the GNPS model has about 3.7dB, 5.8dB, 8.6dB, 10dB, as well as error in QPSK case.

Chapter 5 The performance of the FD models and the TD models

Section 1 compare the GN model family and the Time domain model

In the GN model, we use the different modulation formats, different type of fiber and different distance to simulate, and we get very good results. In the Figure 5.1, even in the ultra long distance between the two extremes, the result of the GN model is almost the same as the model predictions.

In the other hand, there is other important parameter which is optimal transmit power per channel P_{txopt}. We used all the modulations and frequency spacing in SMF and NZDSF(even PSCF, but it is the same as SMF) as the Figure 5.1. The P_{txopt} vs spacing is not depend on model formats. It is matched the model predictions.

However the maximum distance is depended on all the parameter as the Figure 5.1. The simulation curves is proved it. Maximum distance is depended on the increasing of channel numbers. In the model prediction, we use the QPSK in the 32GHz and 50 GHz, the maximum distance will be decrease when the channel numbers increase as Figure 5.1. And the simulation results in the 32GHz and 50GHz can be proved this.

Within EGN models, we used similar way as IGN models to

simulate. The simulation result is more better than GN model as the Figure 5.1. the NZDSF has a error bar in GN model but in the EGN model the error bar has been improved.

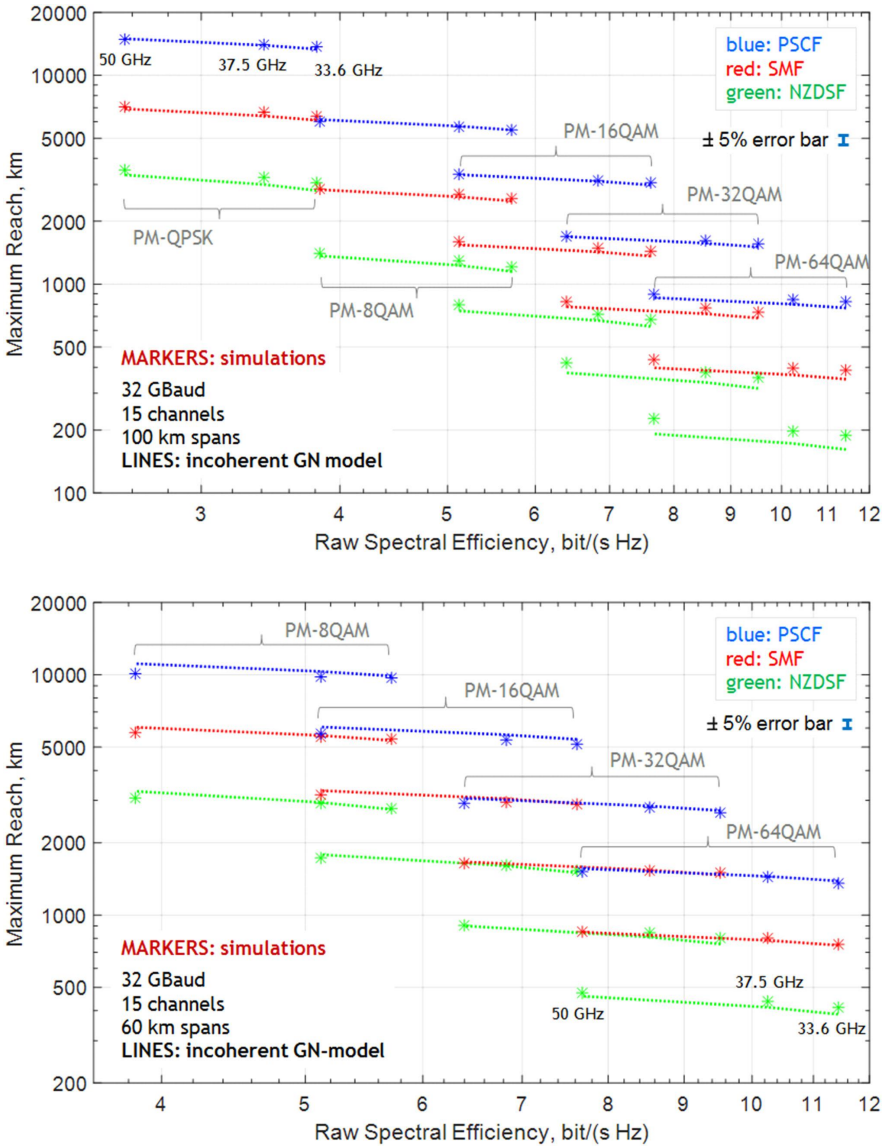

Figure 5.1: Dashed line: predict maximum reach of the system on the basis of the irrelevant GN model, and throughout the whole test 'landscape', every system is configured with raw spectral efficiency with spans of one hundred kilometers (upper part) and sixty kilometers (lower part), respectively. Mark: Simulation outcomes under 33.6, 37.5, together with 50 GHz channel interval(22).

In the time domain model, it find that GN model is not very accuracy. In this model, we use the distance not very long, it is 25km, 50km, 75km

and 100km, the error can be shown in the result which is not acceptable. But it is because the transmission range is very limited. Even in the IGN model, there is a error bar about 5% in the NZDSF, when you decrease the distance, you will find the error bar will be increased to 10%, so you can say it is not suitable in the short range propagation in IGN model, but the signal must be the fully decentralized state in the fiber. And one more, under 500km there will be a large error, but it can use in different accuracy requirements. However in the long distance, more than 500km, this system is much more stable, and can not be depended on the other parameters. So GN model can be acceptable in the NLI noise in the optical links.

Section 2 Compare GN model with the IGN model

In this subsection we separate into two parts, one part is compared about the GN and IGN models prediction for the maximum system reach (MSR) along with the simulation in a very large range of the system configuration. This work provided the first full model performance evaluation.

Within Section 2, several accuracy problems which appear in Section 1 have been investigated by us. In particular, we examine assumption of GN and IGN models described within an attempt to assess the extent to which each one has been validated and which one will lead

to error noticed in Section 1 within this part.

Subsection 1 large range of the system configuration

Three fiber types are used, the parameters of which are shown. They have been particular SMF, big area efficient area PSCF as well as NZDSF. In general, they contain the wide range of dispersion, attenuation as well as nonlinear coefficients. UT test link is uniform and transparent, together with a amplification of concentrated EDFA. The noise diagram of is 5dB.

As a test setup, we pay attention to system on the basis of PM-QPSK, PM-16QAM as well as PM-64QAM (23). In Tx, digital prefiltering is used to get a pulse with square root-bump spectrum, and a roll-off is equivalent to 0.05. The 4 perfect DACs then generate electric signal that drive 2 nesting Mach-Zehnder modulator to work within the linear transfer characteristics. Sign rate (R_s) is set as a 32 GBaud particular business standard value. Channel interval Δf_{ch} spans values as follows: 33.6, 35, 40, 45 as well as 50 GHz(22). The smallest value referring to $1.05 \cdot R_s$ has been the smallest interval even making sure that there isn't any channel-to-channel linear crosstalk, provided selected roll-off. Data is produced adopting several independent PRBSs with length 2^{16}-1, with 4 per PM-QPSK channel, 8 per PM-16QAM channel and 12 per PM-64QAM channel. The PRBS's for each channel is different. The

simulation length is 2^{17} symbols. These lengths have been tested to ensure they have enough Monte Carlo diversity.

By properly adjusting the local oscillator, selecting channel has been implemented within Rx. After light detection was balanced, a Bessel (5-pole) electrical-aliased filter with a bandwidth of $R_s/2$ has been plugged in. The output samples 2 examples per sign. The electronic CD is then compensated by an adaptive 2x2 equalizer, coming with polarization demultiplexing as well as equalization, driven by the least mean square algorithm determined by the equalizer. Since the central channel Tx and local oscillator lasers are considered ideal (no phase noise), carrier and phase recovery are not required. Other channels are sent at five-MHz line-width for a few phase perturbations.

This verification effort has concentrated on making comparison with maximum system-wide (MSR) and model predictions discovered by simulation. The meaning of "MSR" is as follows. The system range (SR) is defined to be the largest quantity of spans which will be obtained when the BER has been lower than the set goal for the given transmit power. MSR has been the largest SR value relative to the transmit power, that is, it is the SR obtained using the best transmit power.

We assume that the system uses FEC with BER equal to 10^{-2}. However, to be realistic, we are not targeting the FEC BER threshold. Instead, our goal is to lower the target BER by 2 dB SNR corresponding

to the FEC threshold, which is considered as an real system margin. The generated aimed BERs are: PM-QPSK, 1.70×10^{-3}; PM-16QAM, 2.04×10^{-3}; PM-64QAM, 2.82×10^{-3}(22). The above BERs have been various due to the various BER-SNR curve slope for every format. To target a rational span number of formats as well as fibers, that it cannot be very big or very small, the length of span is fixed as the various value, decided by the format: 50, 85, and 120 kilometers(22), to PM-QPSK, PM- 16QAM as well as PM-64QAM.

In addition to transmitting the signal before transmitting it to the optical fiber (100000ps/nm), the transmission signal ensures that the signal Gaussian assumption is followed by applying a very substantial per-diffusion (PD). A group of parallel simulations is carried out using the same settings as well.

As mentioned earlier, the simulation is based on a staged algorithm that has been thought to generate a variety of artefact, of which stray FWM. The logarithm approach to alleviate this problem is applied by us. To limit the minimum step size, we simultaneously apply 50 dB of spurious FWM rejection and the largest shift of nonlinear phase, since total instantaneous WDM power accumulated in the 5 ps time window doesn’t exceed 0.1 radian. The numbers have been selected through verification further limiting the precision constraints doesn’t change simulation outcomes.

MSR plot to every setting is presented within Figure 5.2, in which marks have been the simulation outcomes (the circle of non-PD signal as well as the square of the PD signal) and pass GNRF (full line) as well as IGNRF (dotted line). The entire necessary simulation group spent approximately one-year CPU time. GNRF and IGNRF numerical integration was implemented adopting interpreted Matlab code, which has taken several hours on the whole.

The salient characteristic of these figures has been that PD simulation is much closer to GN model prediction and is comparable to the remaining uncertainty of the simulation over the 0.25 dB-error of the fibers, spacing, as well as formats. These results show that the GN model's accuracy is very good while signal-Gaussian assumption has been fully validated. It again highly recommends that the mentioned perturbation as well as AGN assumption must also be sufficiently verified, basically with the best transmit power referring to MSR. While the PD has been taken away, then the system experiences a so-called "initial discrete transient" (IDT), the approximate signal Gaussianity gradually approaches only in this process, with a larger number of errors discovered of GN model and simulation. However, MSR errors never exceeded 0.8 dB in configurations of system. What’s more, GN models seem to be an funny characteristic that is often conserved to non-PD signal, meaning it forecasts that MSR is a bit smaller than simulation shows. It predicts that

the the analog display.

It has been funny that the IGN models seem to produce quite precise predictions for non-PD signal systematically, significantly higher than GN models, as found in previous validation efforts. The outcome has been a bit confusing for IGN models are closer to the models than GN's. Therefore, by principle basically, we can hope the IGN to have a larger error than the GN models.

Certain characteristics of GN and IGN model error which appear in Figure 5.2 has a detailed discussion with following part. However, during this phase, to some extent, both GN and IGN models all seem to efficiently catch the common characteristics of systematic influence from nonlinear circulation, with small false parentheses in a great variety of systems as well as settings.

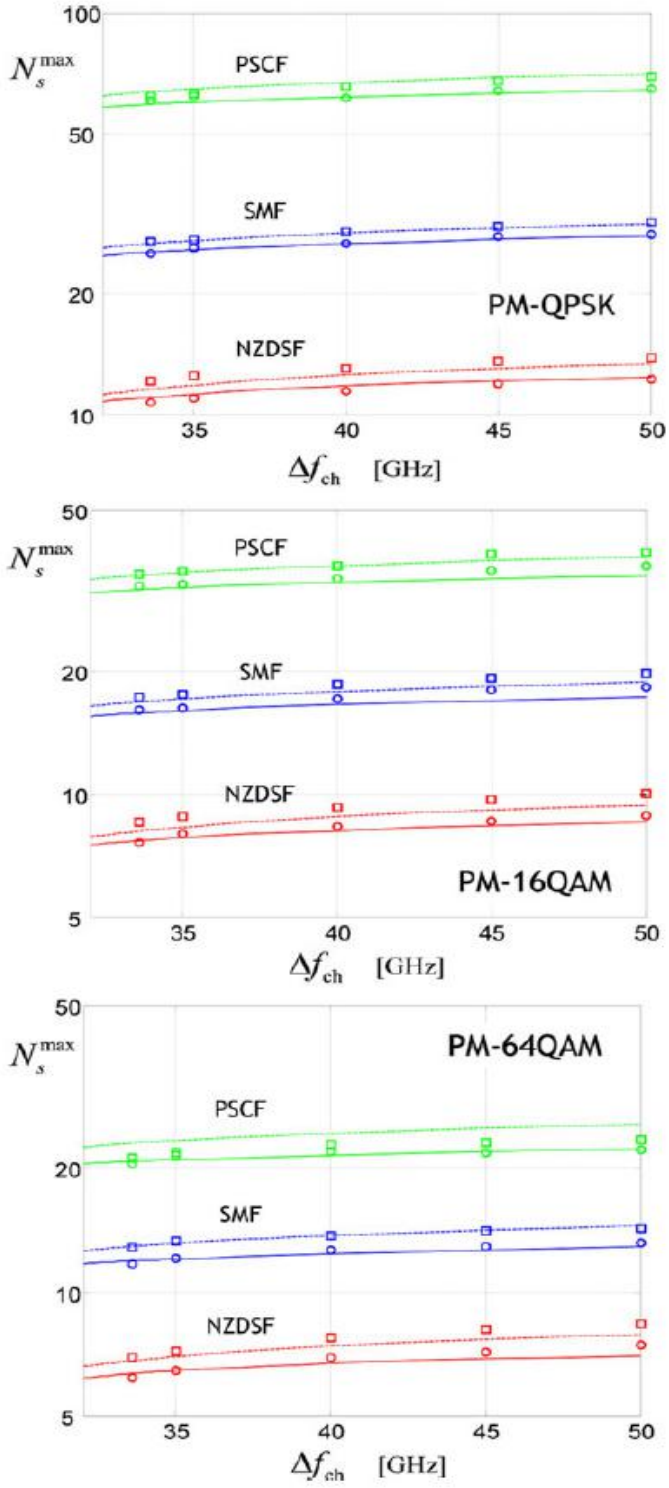

Figure 5.2: Maximum system reach (MSR) diagrams in span number N^{max}s to the test settings, VS. channel interval Δf_{ch} . Upper diagram: PM-QPSK, 120 kilometers of span length . Central diagram: PM-16QAM, 85 kilometers of span length. Lower diagram: PM-64QAM, 50 kilometers of span length. Item in red: NZDSF. Item in blue: SMF. Item in green: PSCF. Full line: predicting GN models. Dotted line: predicting IGN-models. Circle: simulation with great per-dispersion (100,000 ps/nm). Square: simulation with no per-dispersion (22).

Subsection 2 Hypothesis of Perturbative and AGN

When hypothesis of perturbation or AGN fails then the contrast between GN models and the simulation of PD signals will show a substantial error, of course the signal-Gaussian assumption is well validated. In contrast, the results in the former part present outstanding agreement under this situation, which indicates the main inaccuracies for disturbances or AGN hypothesis ought to be excluded.

To be the further specific test for AGN hypothesis, within system simulation shown, the BER are all measured with Monte Carlo direct error counts. Meanwhile, it is calculated with normalized BER formula, adopting SNR to be the direct measure on the signal constellation The average of signal points. When statistic characteristics of the NLI deviate significantly from the AGN, then the analytical formula derived based on the AGN hypothesis will result in a different BER result than the Monte Carlo algorithm(22). Conversely, the consistency of both BER values is often perfectly excellent. It suggests AGN assumption can be considered valid, basically in the perspective of actual system performance assessment. This conclusion is consistent with the previous conclusions drawn from the paper on this issue both in simulation and in experiments.

Subsection 3 Signal-Gaussianity Hypothesis as well as IDT

The truth that GN-model presents with little or without errors in the

PD signal, rather than errors in the PD signal, greatly indicates this will be the signal-Gaussian hypothesis that, in the latter case, it will at least partially fail, requiring careful investigation.

For a specific study of signal-Gaussian assumptions, we focus on evaluating NLI directly, but not evaluating performance parameters related to the system. It is because the latter one usually obscures or suppresses error in NLI evaluation, like what is talked within Section IV-A. Using similar simulation testing format as well as settings stated within the former part, there are only some subtle differences. The setting of Tx spectral roll-off is 0.02 and just 1 interval is adopted: Δf_{ch} = 33.6 GHz, ie $1.05 \cdot R_s$. Length of PRBS increases to 218.1, while total simulation length increases to 218 signs. The analog channel number is 9. The regular and PD signal (200,000 ps/nm predispersed) are started from here. The span length for all settings is set to 100 km. Regarding step-by-step parameters, fake FWM repression is set as fifty dB, while the largest non-linear phase shift is fixed at 0.025 radian.

Section 3 Compare GN model with the EGN model

Jus like what we talked before, the bad performance at low sign rate is one of the disadvantages for GN models. The truth that GN models demand the fully decentralized signals for working correctly is able to explain this situation, which has been an essential (although not enough)

condition to signal Gaussian approximation. The EGN model eliminates the Gaussian approximation of the signal, so it can be inferred that small dispersive signals are well implemented even at low symbol rates.

Prior to the test this hypothesis, we want to show the preciseness at low sign rate seems to be essentially a no meaningful academic subjects, as if, all of the symbol rate in the field of optical communications have been steadily rising. In particular, the current 32GBaud industry standard seems to soon be replaced by new systems running at speeds up to 64GBaud and beyond, paying attention to the latest news release as well as the announcement from the main suppliers..

Surprisingly, however, higher symbol rates appear to have some inherent nonlinear losses and lower loss rates. In some cases, this punishment can be substantial. This led to a set of electronic sub-carriers proposed to generate a system of new higher sign rate to be a DAC, each operating at the best symbol rate in NLI mitigation. Such a conception is called "symbol rate optimization" of the "SRO" .

Please note within the article we show no interest in SROs. Instead, we intend to explore the entire range of the effectiveness of the non-linear model. In addition, we think it is vital to show precisely simulating NLI with a low sign rate isn’t only an interest in academic research. It is likely to become an important aspect in practice as well.

For the purposes of this study, the symbol rate R_s per channel varies,

when other major system characteristics remain unchanged.

In particular, we impose:

1) Total optical bandwidth BWDM

2) Relevant channel interval $\delta f = \Delta f / Rs$

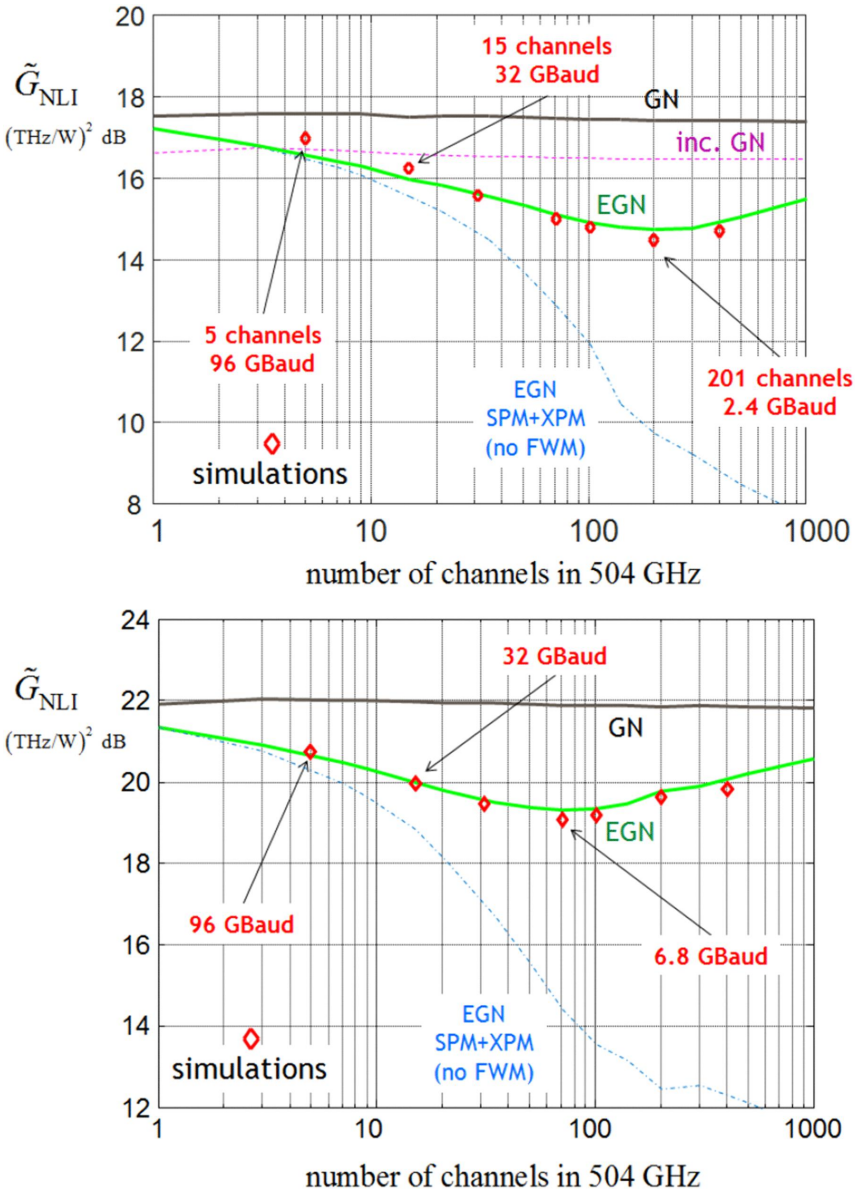

Fig 5.3: Standardized average NLI noise power spectral density *G*NLI on middle channel, vs. the channel number within the set total WDM bandwidth with 504 GHz. PM-QPSK modulation, quasi-Nyquist: roll-off 0.05, interval 1.05 times the sign rate. Measure NLI at 50-span SMF (upper part) or 30-span NZDSF (lower part). Line: computation adopting the model suggested within the diagram.

Mark: simulation (22).

These 2 parameters set decide spectral efficiency in the system as well as the total (original) bit rate, separately:

$$S = \frac{b_s}{\delta f} \quad (5\text{-}1)$$

$$R_{b,tot} = B_{WDM} \cdot S \quad (5\text{-}2)$$

where bs is the bit number per sign. It is assumed that: B_{WDM} = 504 GHz, ρ = 0.05, δf = 1.05 together with PM-QPSK transmission (b_s=4)(23). The generated spectral efficiency as well as total original bit rate has been S = 3.81 b/(s·Hz) and $R_{b,tot}$ = 1.92 Tb/s.

Like what has been described above, as a free parameter, there is apparent limitation with R, which must divide WDM bandwidth into multiple channels provided by:

$$N_{ch} = \frac{B_{WDM}}{(1+\rho)R_s} \quad (5\text{-}3)$$

It must be an integer. We should notice when the value R_s =thirty-two GBaud has been selected, and function (5-3) accurately generate N_{ch} = fifteen channels and, In this case, the system settings are consistent with the system settings used in Landscape for gaining the data point to the PM-QPSK within 33.6 GHz channel interval(22).

In the output of connection, NLI power P_{NLI} was measured by us at the WDM comb center channel (CUT). But only making comparison with

P_{NLI} in system which adopts various sign rates won't provide data about the relevant MR performance at once. Therefore, we get in P_{NLI} an appropriate amount of standardization we call G_{NLI}:

$$\widetilde{G}_{NLI} = \frac{P_{NLI}}{R_s G_{ch}^3} \qquad (5\text{-}4)(22)$$

Where G_{ch} is the transmitted signal PSD averaged over the average WDM signal on the flat top of all transmitted channels. G_{NLI} can be thought of to be $G_{NLI}(f)$ average impinging upon CUT, normalizing cubes relative to G_{ch}.

G_{NLI}'s major features are as follows: In systems using different symbol rates, the same G_{NLI} value means they can reach the same maximum range. This makes G_{NLI} at different symbol rate performance is very convenient. Figure 5.3 plots G_{NLI} as a marker for the channel number split for the set BWDM optical bandwidth up for an SMDS being taken measurement in fifty spans (upper part) to NZDSF being taken measurement in thirty spans (lower part). The outcomes obviously suggest the G_{NLI} isn't a constant , but in fact gets an amino value of approximately 2.4 GBaud as well as 6.4 GBaud, separately. To approximate resolution for the best sign rates.

For GN model (consistent and inconsistent), none of them can catch the G_{NLI} declining as the symbol rate drops. On the SMF Figure 5.3 (upper part)), consistent GN models (dotted lines) operate very closely to

the simulation in the 32 to 96 GBaud range. However, the G_{NLI} level in the best sign rate has been almost 2 dB. GN model even farther. In both fibers, the EGN model is simulated very closely throughout the test interval. It makes accurate prediction on the best sign rates as well as the relevant values

Another curve has been increased by us, the EGN model curve without FWM contributions, as the FWM will always be ignored within the modeling files because it can be ignored with high sign rate. These figures suggest ignoring FWM at high symbol rates yields sufficiently accurate results, but this approximation is not plausible at low sign rate. Especially, ignoring FWM won't generate the smallest G_{NLI} because FWM-free curves steadily decay while decreasing and decreasing the symbol rate.

More similar to Figure 5.3 can be found , along with actual MR simulation tests validated for NLI mitigation, gained through the optimization of sign rates.To sum up, EGN models seems to be reasonably dependable at every sign rate, though the signal is essentially un-distributed or even very low. So it is able to be applied to studying multiple sub-carrier systems, especially to the SRO evaluation.

Let's come to the final conclusion, it can be seen from Figure 5.3 that GN model accuracy again increases toward the typical super low sign rate (no more than one GBaud) for OFDM system. It is because OFDM

signal is likely to inherently present the joint Gaussian population since they have been divided into many an independent sub-carrier.

Chapter 6 Validation of the quality of transmission

Today, the demand for data and the speed of traffic are increasing rapidly. In the future, into the 5G era, virtual reality and cloud services will also develop rapidly, and very large bandwidth will be needed on the backbone optical network. In this paper, we present a physical simulation environment for open optical transmission on telecommunications infrastructure projects for the design and operation of transmission quality assessments.

Section 1 Merit of the Raman amplification and Generalized GN-model

Subsection 1 Raman merit

According to (37), we solve the transparent and re-configurable optical network, and use EDFA to upgrade the capacity of the optical link. The best method is the Raman pump of the opposite propagation, the highest Raman gain can be Up to 60%. This scheme is also the best power effectiveness as well as being steady for alterations in total input power because of the increase/decrease on the channel. When Af = 30 dB, the OSNR increases with the loss of fiber spans to approximately four dB.

Such as, we used three fiber types to test Raman performance, so as to explore the RA percentages(can reach one hundred percent along with various pumping plans. The fiber span loss between 20 and 30 dB was studied by us. The answer is that based on full Raman gain pumping, all fiber performance is similar, with no outstanding performance and best performance, for example, with a 25% co-propagation pump and a 75% back-propagation pump. This configuration increases the Raman performance of the NZDSF to 5.9 dB(37) at a fiber span loss of 30 dB.

Subsection 2 The Optical Link Emulator

In the previous chapters, we consider NLI as Gaussian noise. By (39), we consider NLI as generalized Gaussian noise, including the spectral variation of SRS and its gain/loss. In (39), we built a GGN model to test whether the QoT Estimator performance based on this model is accurate, compared to a commercial device including a 100Gb/s transponder. We have shown that the results of the two methods are consistent within a signal-to-noise ratio error of 0.5 dB, indicating that GGN models will be applied to many types of QoT estimators. In addition, GGN models show their ability on prediction of spectrum tilt because of SRS within SNR performance, allowing it to assess linear pre-tilt effects on SRS per-making up as well as generation of NLI.

After these analysis and evaluation in (38), we created a QoT

calculator within PSE frame, called the OLE API of OLE. OLE construction has been stated within flow chart in Figure 6.1. OLE demands 2 input data groups: one is a statement on physical layer, while the other is the group of spectrum data. Statement on physical layer represents the topology data for the route being tested, ie link description including the description in detail about the network components divided into 3 types: fiber span, amplifier as well as passive components. The spectrum data demands detailed information on power spectrum density in the WDM channels and/or super-channel comb circulating on analyzing path, containing the changes that may be led through ROADM traversing the path and the definition for WDM channel plan being adopted, for channels The power allocation affects NLI numbers on each channel. Once the input is set, the OLE engine will run the modules associated with every one within 3 types of network elements and sort and initialize them according to the link description. The module considers the channel, ASE noise and NLI spectrum at its input, applies frequency related gain or loss and generates an outputting spectrum. Fiber optic modules operate GN models while extending signal, evaluating NLI amount produced from fiber spans as well as upgrading NLI spectra. Amplifier modules will amplify signals according to the given gain together with noise numbers distribution map, calculates referring amount of ASE noise generation, and updates the ASE noise spectrum

accordingly. Passive element has been the plain attenuator. If route being analyzed is fully passed, a common SNR can be used for each channel. With the aims of routing as well as designing, using the most terrible case transferring assumption-scan run OLE (ie assuming full spectrum loading of each fiber link).

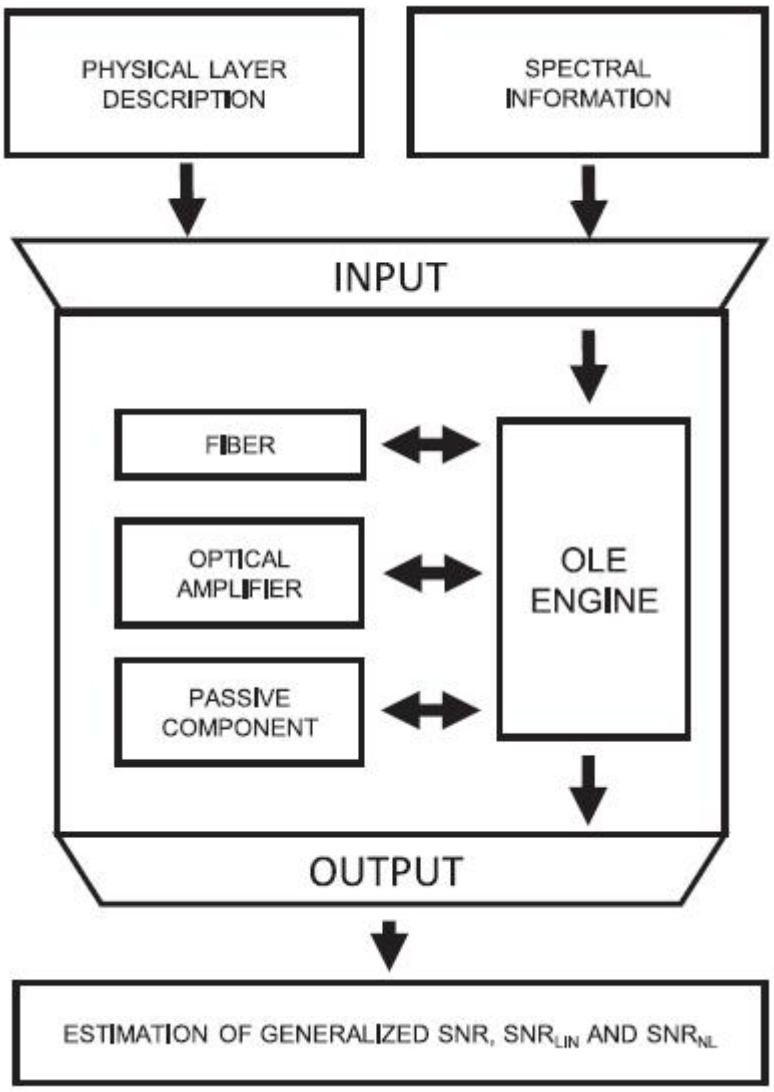

Figure 6.1：Structure of the OLE (38)

Section 2 Structure of the quality of transmission laboratory system

In this section, I will introduce two laboratory according to (38)(39) which in based on Microsoft Labs and Corning SSMF-28e+®

The first one is as shown in Figure 6.2. It is connected by the Open Line System (OLS) that connects the hybrid fiber network path consisting of commercial device with a circulation distance reaching 1,945 kilometers.

OLS has the oriented structure without color and fully supports SDN support within exotic wavelength. Most of NZ-DSF fiber plants span 1,945 kilometers in both directions, consisting of approximately 85% of Corning LEAF as well as fifteen percent of Corning SSMF-28e+®. Every ROADM has been configured with the boost amplifier together with the preamplifier. 8 various consistent modem vendors took part in studies - Juniper, Arista, Ciena, Coriant, Acacia, Cisco, Infinera, as well as Nokia - offering a consistent source across various optical processing technologies along with specific DSP complements (32 total)) (within thirty-two sources, representing 5 specific DSP complements). The parameters can refer to the section in(38).

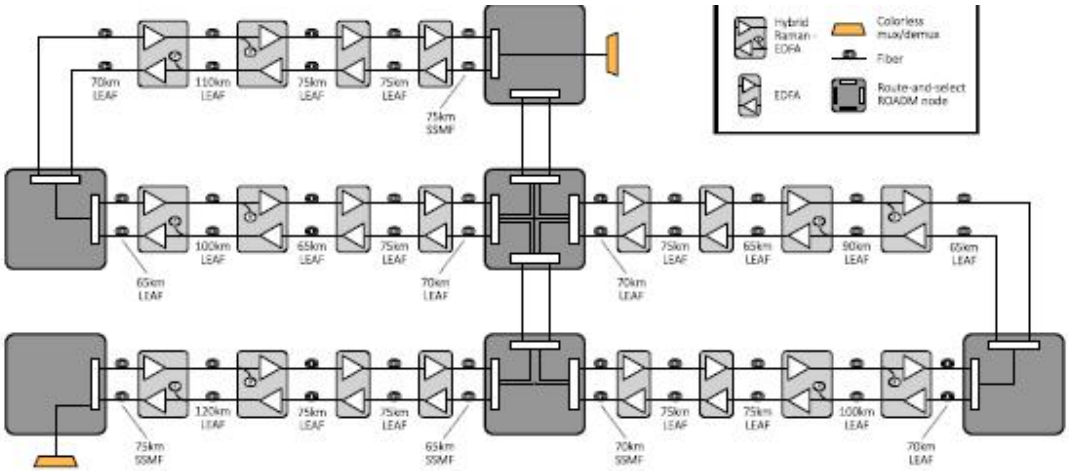

Figure 6.2：Microsoft Lab's test platform

The second one is the Orange Lab test platform is used, as shown in Figure 6.3. It consists of 20 eighty-kilometer Corning SMF-28e +® fibers. It has been especially adopted to evaluate transponder performances deployed within an Orange network.

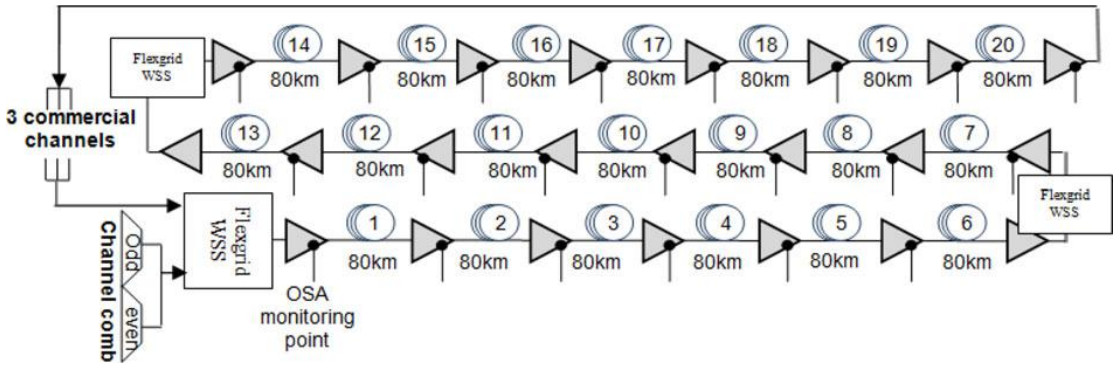

Figure 6.3: Structure of the Orange network (39)

Section 3 Validation and result

The method used in the(38) during the test bench measurement is as follows. Light sources from eight vendors use back-to-back noise load settings that capture the BER versus OSNR of every equipment upon the best receiving power (the receiving power set-points are also reserved for propagation measurements). Then, the measured bandwidth is normalized by using the symbol rate of the coherent source, the OSNR value from the measurement is converted to a linear SNR value, and then the relation of BER performances together with SNR is obtained. Then, the ninety-four channels circulated around fiber test bed as well as capturing the BER when scanning the full 1945 km of light emission power. This process is repeated with central distances in 410, 800, 1165 as well as 1540 kilometers.

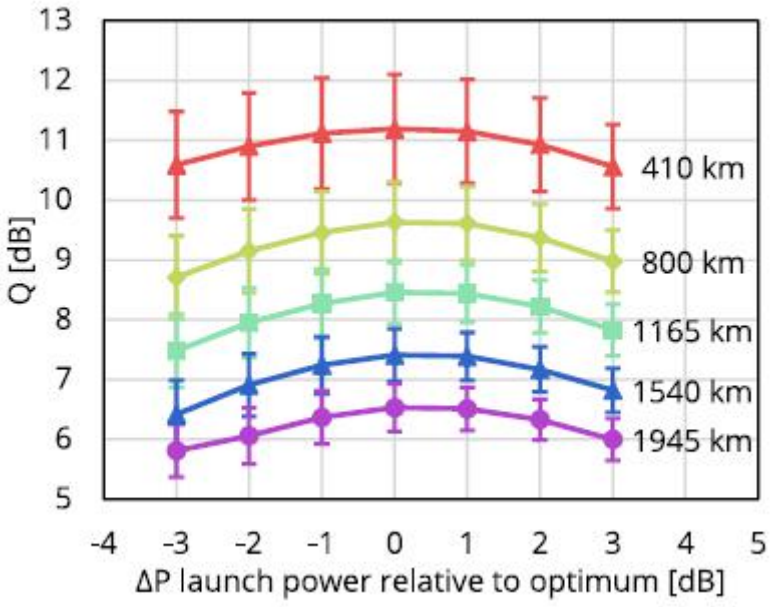

Figure 6.4: Performance of Q-factor (38)

As shown in Figure 6.4, the curve shows the Q-factor average performance of all commercial sources, although the DSP implementation is different, but the best channel transmit power is found to be no more than 0.5 dB from each other. The back-to-back BER of each source is compared to the (linear) SNR characteristics. By adopting this method, BER value is reflected to the referring SNR value (including linear-nonlinear noises) for comparison on software output. The reflection will be effective, supposing no dispersion and non-linear losses in various DSP complements.

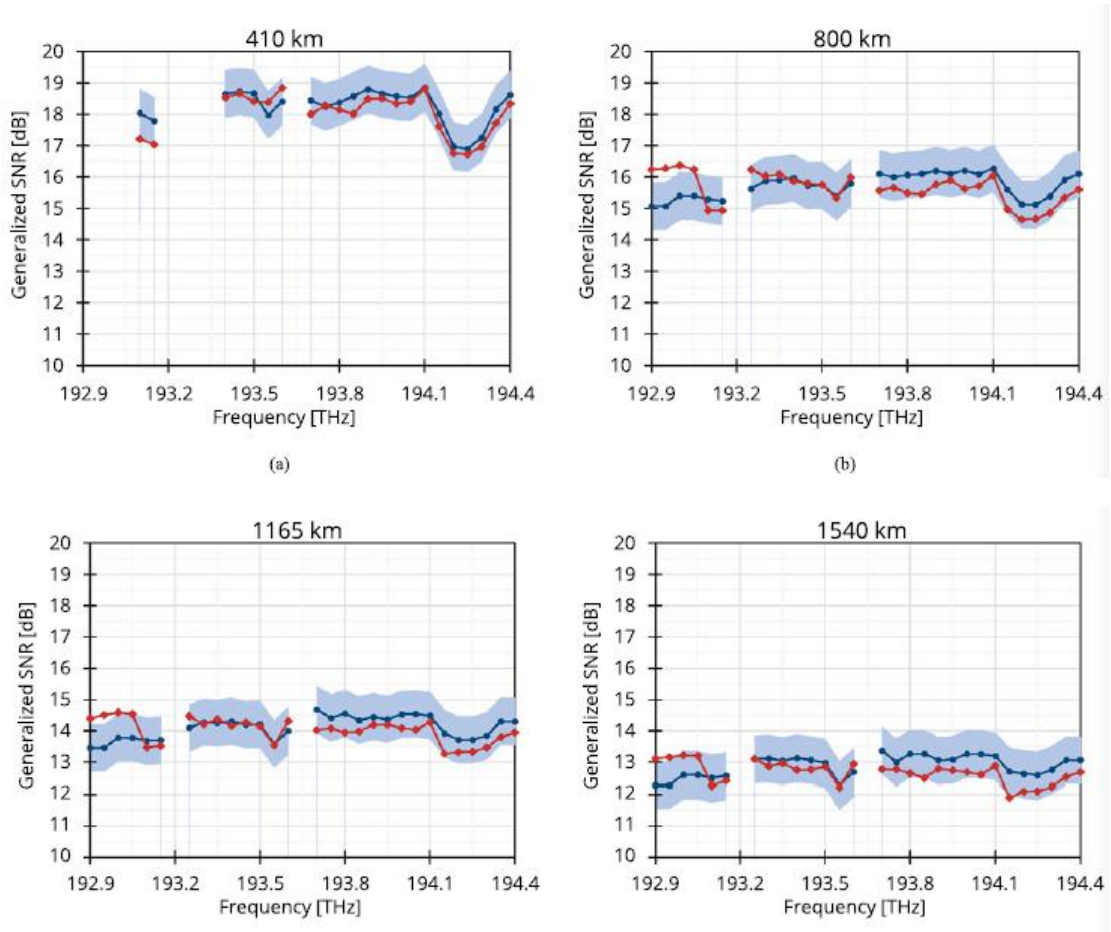

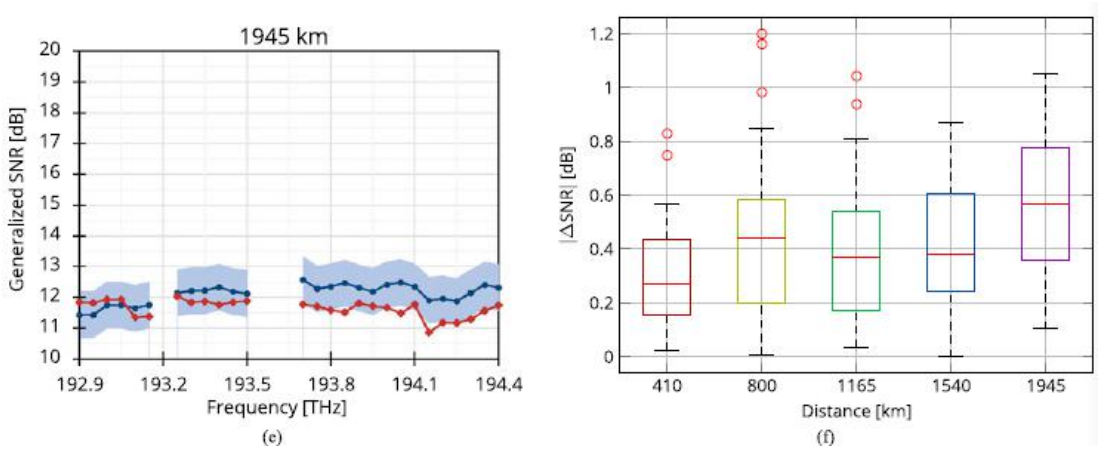

Figure 6.5: (a)to (e) presents SNR measurement (diamonds mark curve in red) as well as the estimated value ±0.75 dB (dot mark curve in blue) versus frequency of 27 center frequency values for commercial line card adopted in comparing. (f) presents a box chart of relationship between the absolute values in estimated errors and the space.(38)

Within Figure 6.5(a), low frequency point has been ignored because they require too much B2B measurement inference for estimating the generalized SNR value. Within Figure 6.5(e), since signal degradation is too high, the state is deactivated at 193.55THz and 193.6THz, so the BER before FEC cannot be used. In the Figure 6.5(f) Because it modifies the attenuated fibers along fiber's every channel based on PSD of input. The influences describe the reason that OLE estimation on most channels is not conservative with respect to SNR measurements, and the reasonable assumption can be made on that the influence may be resulted from the truth that in practical systems, large-capacity modulation sources are independent and identical. The distributed source has a lager degree with connection, while the ASE channel is more disturbing than the data channel. Carry the signal. Finally, in terms of estimation accuracy, the error distribution is consistent with the OOPT-PSE goal. This increase in

the ΔSNR median and distance is due to the accumulation of errors. These issues represent the direction of OLE development.

In the second experiment, we validated QoT-E for the first time through making a comparison between the predictions with measurements upon 6 channels produced on the test platform by commercial lab-based business one hundred Gb/s transponders in Orange Labs. Use of medium GGN model.

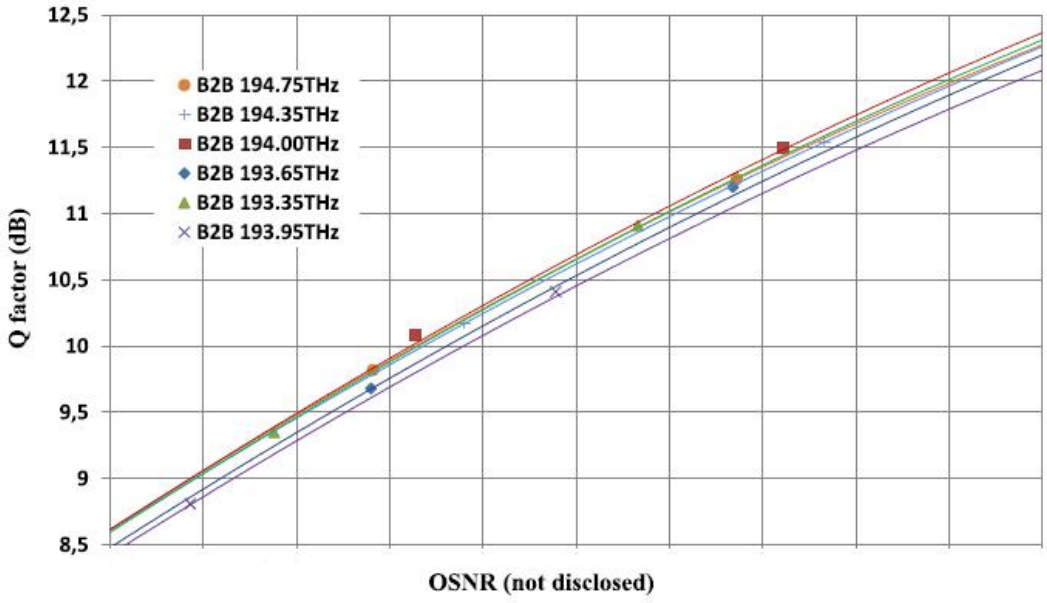

Figure 6.6: back-to-back (B2B) Q-versus-OSNR (5)

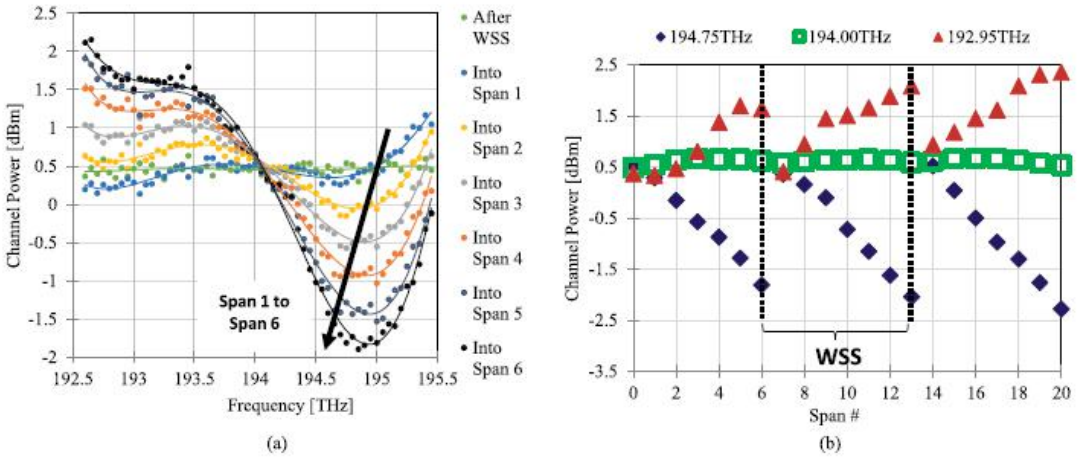

Figure 6.7: Power progress because of SRS as well as ripples of amplifier along Orange test beds.(39)

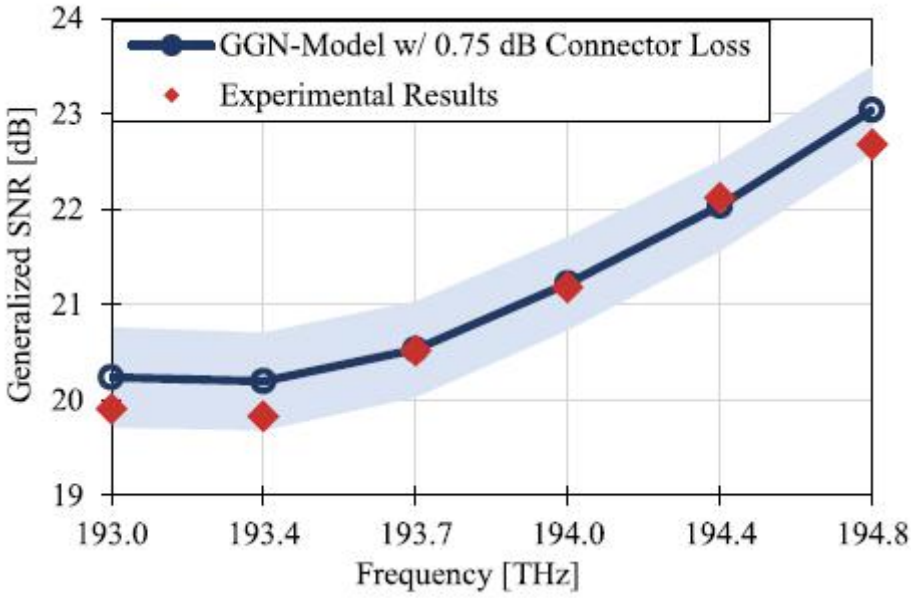

Fig. 6.8：Comparing nonlinear SNR in experiment as well as modeling(39)

Verification shows outstanding agreements of QoT-E prediction as well as measurement, which can quantitatively provide the QoT-E reliability scope in ±0.5 dB to the measurement channels. This refers to that within this setting, using Qot-E prediction on the basis of the GGN model, the margin of the optical path can be restricted to 0.5 dB without considering spectrum position in transferring bandwidths. So the outcomes of verification in the experiments inspire using GGN models within the QoT-E module required for network design for several vendors as well as arrangement because it provides consistent QoT estimates throughout the WDM spectrum. To do this, it is necessary to follow the same method used in the acquisition (for obtaining an approximation of the GN model) for deriving the approximate closed form to GGN models.

Chapter 7 Conclusion

In this thesis we gather all the outcomes of GN model family as well as introducing the application and knowledge. We are focusing on the key point of the simulation result and give some disadvantages and error for the GN model. In general, GN model in the UT transmission system is perfect and can be used in many applications. There are some error which we found in the result because of the Gaussian approximation, this will let the accuracy is very low in the short range transmission or in the beginning of the UT links, in the recently research, many paper want to find a way to improve the performance without increase the complexity in model. By the way, the EGN model usually have a better performance than GN model which means have less error. This is very significant for us to predict system performance and actual system configuration.

We also collect many simulation result about the close from of the GN model in order to show the accuracy and the limitation. Finally we describe many application used by GN model, and these model are used the closed-form approximate settlements. Our analysis on the throughput together with optimization, we can find which parameters can influence the performance in order to derive the approximate "design rules". This extensive result can approve that non linear interference model is usable and widely influential. Finally we can make sure that GN models used for

generating the entire optimization and controlling strategies upon next-generation optical routing networks. Now about the model, researching is continue to find a new and better model and optimized the GN model. In this background, we think now the GN model is the easy stable to have a good performance and accuracy. In general, we find now The outcomes for the latest modeling efforts fundamentally improved common knowledge of the performance of a UT optical system and the method they are analyzed and designed. We will build better models in the future to improve the overall optimization and control strategy of optical routing networks.

Acknowledgment

First and foremost, I would like to express my deepest gratitude to my supervisor, Prof. CURRI VITTORIO and co-supervisor, Dr. PILORI DARIO and Dr. CANTONO MATTIA , who have provided me with valuable guidance in writing this thesis and offered precise modifications and comments. Without their instruction, kindness and patience, I could not have completed my thesis. I also would like to show my thanks to my family and my friends for their encouragement and support during my study.

Bibliography

(1) www.optcore.net

(2) University of Babylon

(3) www.scribd.com

(4) www.cables-solutions.com

(5) Carena, A., V. Curri, G. Bosco, P. Poggiolini, and F. Forghieri. "Modeling of the Impact of Nonlinear Propagation Effects in Uncompensated Optical Coherent Transmission Links", Journal of Lightwave Technology, 2012.

(6) University of Nottingham

(7) Oklahoma State University

(8) www.ceid.upatras.gr8

(9) Tang, J.. "Optical nonlinear effects on the performance of IP traffic over GMPLS-based DWDM networks", Computer Communications, 20030721.

(10) d-nb.info

(11) Seiji Norimatsu. "Statistical evaluation of transmission performance degradation originating with cross-phase modulation", Electronics and Communications in Japan (Part I Communications), 01/2007.

(12) Nanyang Technological University

(13) soe.northumbria.ac.uk

(14) Morio Kobayashi. "Optical demultiplexer using coupling between nonidentical waveguides", Applied Optics, 10/15/1978.

(15) University of Technology

(16) Universiti Putra

(17) www.sopto.com

(18) dspace.kuet.ac.bd

(19) L.C. Calmon. "SRS and XPM in multiamplified optical systems with DS fibers in 10 Gb/s", 1999 SBMO/IEEE MTT-S International Microwave and Optoelectronics Conference SBMOMO-99, 1999.

(20) INTI International University

(21) www.eng.tau.ac.il

(22) Poggiolini, Y. Jiang. "Recent Advances in the Modeling of the Impact of Nonlinear Fiber Propagation Effects on Uncompensated Coherent Transmission Systems", Journal of Lightwave Technology, 2017

(23) Porto.polito.it

(24) University College London

(25) P. Poggiolini, G. Bosco, A. Carena, V. Curri, F. Forghieri. "A simple and accurate model for non-linear propagation effects in uncompensated coherent transmission links", 2011 13th International Conference on Transparent Optical Networks, 2011

(26) Dar, Ronen, Meir Feder, Antonio Mecozzi, and Mark Shtaif. "Properties of nonlinear noise in long, dispersion-uncompensated fiber links", Optics Express, 2013.

(27) Carena, A., V. Curri, G. Bosco, P. Poggiolini, F. Forghieri. "Modeling of the Impact of Nonlinear Propagation Effects in Uncompensated Optical Coherent Transmission Links", Journal of Lightwave Technology, 2012.

(28) Dar, Ronen, Meir Feder, Antonio Mecozzi, and Mark Shtaif. "Accumulation of nonlinear interference noise in fiber-optic systems", Optics Express, 2014.

(29) Queen Mary and Westfield College

(30) Xavier Litrico, Vincent Fromion. "Modeling and Control of Hydrosystems", Springer Nature, 2009

(31) docplayer.ru

(32) P. Poggiolini, G. Bosco, A. Carena, V. Curri, Y. Jiang, F. Forghieri. "The GN-Model of Fiber Non-Linear Propagation and its Applications",Journal of Lightwave Technology, 2014

(33) P. Poggiolini, Y. Jiang, A. Carena, G. Bosco, F. Forghieri. "Analytical results on system maximum reach increase through symbol rate optimization", Optical Fiber Communication Conference, 2015

(34) Min Tao. "Recovering Low-Rank and Sparse Components of Matrices from Incomplete and Noisy Observations", SIAM Journal on Optimization, 2011

(35) Hadjidimos, A.. "Nonoverlapping domain decomposition:", Mathematics and Computers in Simulation, 200002

(36) van Breugel, F.. "Domain theory, testing and simulation for labelled Markov processes", Theoretical Computer Science, 20050301

(37) Vittorio Curri, Andrea Carena, "Merit of Raman Pumping in Uniform and Uncompensated Links Supporting NyWDM Transmission" JOURNAL OF LIGHTWAVE TECHNOLOGY, VOL. 34, NO. 2, JANUARY 15, 2016

(38) Mark Filer,Mattia Cantono ,Alessio Ferrari, Gert Grammel, Gabriele Galimberti, Vittorio Curri "Multi-Vendor Experimental Validation of an Open Source QoT Estimator for Optical Networks" JOURNAL OF LIGHTWAVE TECHNOLOGY, VOL. 36, NO. 15, AUGUST 1 2018

(39) Mattia Cantono ,Dario Pilori , Alessio Ferrari, Clara Catanese, Jordane Thouras, Jean-Luc Auge´, Vittorio Curri "On the Interplay of Nonlinear Interference Generation With Stimulated Raman Scattering for QoT Estimation" JOURNAL OF LIGHTWAVE TECHNOLOGY, VOL. 36, NO. 15, AUGUST 1, 2018

(40) Mattia Cantono, Jean Luc Auge, Vittorio Curri “Modelling the Impact of SRS on NLI Generation in Commercial Equipment: an Experimental Investigation” OFC 2018 © OSA 2018

(41) Vittorio Curri, Andrea Carena, Pierluigi Poggiolini, Gabriella Bosco, Fabrizio Forghieri “Extension and validation of the GN model for non-linear interference to uncompensated links using Raman amplification” ©2013 Optical Society of America

(42) Pierluigi Poggiolini. "The GN Model of Non-Linear Propagation in Uncompensated Coherent Optical Systems", Journal of Lightwave Technology, 2012